
Abstracts for the Planetary Geology Field Conference on Aeolian Processes

Ronald Greeley and David Black
January 1978

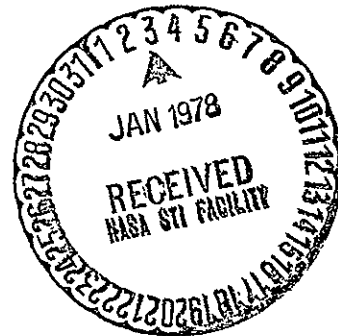
(NASA-TM-78455) ABSTRACTS FOR THE PLANETARY
GEOLOGY FIELD CONFERENCE ON AEOLIAN
PROCESSES (NASA) 63 p HC A04/MF A01

N78-13492

CSCL 08G

Unclas
55195

G3/42



NASA

National Aeronautics and
Space Administration

Ames Research Center
Moffett Field, California 94035

Abstracts
for the
PLANETARY GEOLOGY FIELD CONFERENCE
on
AEOLIAN PROCESSES

Ronald Greeley, Editor
Department of Geology and
Center for Meteorite Studies
Arizona State University
Tempe, Arizona

and

David Black, Coeditor
Space Sciences Division
Ames Research Center-NASA
Moffett Field, California

January, 1978

TABIE OF CONTENTS

| | page |
|---|------|
| 1 Ahlbrandt, Thomas S , Andrews, Sarah, and Fryberger, Steven S Effects of Cold Climate on Eolian Deposits. | 1 |
| 2. Arvidson, R., Carlston, C , Guinness, E., Jones, K., Pidek, D , Sagan, C , and Wall, S. Constraints on Aeolian Phenomena on Mars from Analysis of Viking Lander Camera Data. | 3 |
| 3 Bagnold, Ralph A Wind - Sand Interactions | 8 |
| 4 Breed, Carol S , McCauley, John F , Ward, A Wesley, and Fryberger, Steven G Dune Types and Distribution in Sand Seas, Earth and Mars | 9 |
| 5 Breed, William J and Breed, Carol S Star Dunes as a Solitary Feature in Grand Canyon, Arizona, and in a Sand Sea in Sonora, Mexico .11 | .11 |
| 6. Dzurisin, D Aeolian Stripping of Ash Layers in Kau Desert, Kilauea Volcano, Hawaii | 13 |
| 7. Forsman, N.F. Experimental Eolian Erosion by Very Fine Grains at Terrestrial and Martian Atmospheric Pressures | .14 |
| 8. Fryberger, Steven G and Ahlbrandt, Thomas S Techniques for the Study of Eolian Sand Seas | .16 |
| 9 Gillette, D Tests of a Portable Wind Tunnel for Determination of Wind Erosion Threshold Velocities | 18 |
| 10 Greeley, Ronald, Spudis, Paul, and Johannesen, Dann Geology and Aeolian Features of the Hellas Basin Floor..... | .19 |
| 11. Haynes, C V. The Nubian Desert A Product of Quaternary Climatic Cycles | .22 |
| 12 Iversen, J D. and Greeley, Ronald Comparison of Wind-Tunnel- Model and Atmospheric Full-Scale Experiments of the Amboy Crater and Adjacent Topography | 24 |
| 13 Kieffer, Hugh H and Palluconi, Frank Don Martian Surface Partical Sizes Determined by Thermal Mapping | .27 |
| 14 Krinsley, David H and Greeley Ronald. Surface Textures of Sand Sized Particles abraded under Earth and Martian Conditions | 30 |
| 15 McCauley, Camilla K and Cotera, Augustus S Eolian Deposits of Paiute Trail Point, Arizona. | .33 |
| 16 McKee, Edwin D. Interpreting Dune Deposits Through Minor Structures. .,35 | .35 |
| 17 Peterfreund, Alan R Dust Storms on Mars Visual and Thermal Observations from Viking | 37 |
| 18 Pollack, J B. Viking Observations of Dust Suspended in the Martian Atmosphere | 40 |

| | | |
|-----|---|----|
| 19 | Smith, Roger. Barchan Dunes Development, Persistence and Growth in a Multi-directional Wind Regime, Southeastern Imperial County, California.. .. . | 42 |
| 20. | Smith, Roger. The Algodones Dune Chain, Imperial County, California.. .. . | 43 |
| 21. | Thomas, P , Veverka, J., and Gierasch, P Mars· Frost Streaks in the South Polar Cap.. .. . | 45 |
| 22 | Veverka, J., Thomas, P , and Bloom, A Classification of Martian Wind Streaks | 46 |
| 23 | White, B R. and Greeley, R. Wind Transport Rates on Mars . | 48 |
| 24 | White, Bruce R , Iversen, James D., and Leach, Rodman N. Wake of a Three-dimensional Disturbance in a Turbulent Boundary Layer | 52 |
| 25 | El-Baz, Farouk. Apollo-Soyuz Observations of Desert Environments. . . . | 57 |

EFFECTS OF COLD CLIMATE ON EOLIAN DEPOSITS

Ahlbrandt, Thomas S., Andrews, Sarah, and Fryberger, Steven G., U.S. Geological Survey, Denver, CO 80225.

Extended periods of sub-freezing temperatures combined with precipitation may modify eolian deposits in at least four ways: (1) reduce the rate of dune migration, (2) deform stratification by the melting of snow layers, (3) develop dissipation structures by infiltration of meltwater, and (4) produce and preserve minor structures that normally would be destroyed. These observations were made from studies of the Killpecker dunes, Wyoming; Nebraska Sand Hills; North Park dunes, Colorado; and Great Sand Dunes, Colorado; that took place during the past seven years.

The periodic freezing of moisture in cold-climate dunes slows dune movement to a rate approximately one order of magnitude less than that expected for dunes of warm climates and equivalent wind regime. Wind regimes are compared using a sand rose technique developed by Fryberger. For example, dunes in North Park, Colorado, migrate less than 2 meters per year, as measured in sets of aerial photographs spanning 30 years, even though the dunes occur in a unimodal, high-energy wind regime. The freezing of moisture in dunes, or snow cover, virtually immobilizes the North Park dunes during the winter months of high wind energy.

Melting of snow that has become interlayered with sand is a mechanism that produces deformed stratification in cold-climate dunes. As snow melts, tensional structures develop in the upslope portions of overlying sand layers, and these subside to fill the space formerly occupied by snow. In contrast, compressional structures form on the downslope margins of overlying sand layers within the contorted zone. Deformed strata created by the melting of snow may range in thickness and length from several centimeters to several meters. The degree of deformation produced by snow melt and subsequent collapse of overlying sand increases roughly in proportion to increase in thickness of the snow layer. This increase results from greater volume loss.

Snow-melt deformation is most common on the lee sides of dunes, generally in slipface deposits. We have observed snow-melt deformation in lee-side deposits of dome, transverse, barchan, parabolic, and reversing dunes. Within the slipface, the snow layers are generally thickest near the brink of the dune and are thinner downslope; they have a flat base and convex-upward upper surface. The convex-upward profile of the snow layers intensifies deformation of overlying sand. As the snow melts, sand overlying the thickest part of the snow layer drops farther than sand covering thinner parts. The snow-melt deformation occurs mostly in sand made cohesive by infiltrating meltwater. Snow-melt deformation preferentially develops as isolated features near the tops of crossbed sets; these features contrast with loading deformation features commonly formed near the base of crossbed sets.

Dissipation structures, a type of contorted bedding, have been observed to form in warm-climate dunes following heavy rainfall (Bigarella, 1975) or by pedogenetic processes. However, in cold-climate dunes they form by a different process. Dissipation structures are superimposed on original

eolian stratification. They consist of discontinuous, dark bands that have a higher content of fine-grained material, predominantly clay, than adjacent layers. Above frozen sand layers in cold-climate dunes, dissipation structures may form when clay is deposited along the impermeable upper margin of the ice by downward percolating meltwater. Frozen layers of sand may be intercalated with non-frozen layers to considerable depths beneath the snow layer. Textural analyses demonstrate that the upper surface of frozen sand layers may be enriched in fine-grained material, especially clay. The local source of the clay in dissipation structures is probably clay coatings, dominantly montmorillonite, which is common on the eolian sand grains in the dune fields studied.

The surface of sand upon which snow rests on a dune may also be altered. Initially smooth sand surfaces buried by snow become pitted when the snow melts. The pits give a dimpled appearance to the sand but do not have the raised rims and depressed centers of impact structures such as raindrop and hail imprints. The freezing of sand surfaces increases the chance of preservation of surficial features such as bioturbation traces and ripple marks. Frozen surfaces on the slipfaces of dunes have been observed to be buried by sand derived from the windward slope, thus preserving these surficial features.

The reduction in rate of sand movement in the cold-climate dune fields we have studied suggests that new interpretations are necessary for dynamic measurements of dunes that receive sufficient precipitation to form ice or snow. The association of isolated deformation structures in the upper parts of crossbed sets, dissipation structures, and pitted bedding-plane surfaces are indicators of cold-climate processes which should be differentiable in eolianites.

REFERENCE CITED

- Bigarella, J. J., 1975, Lagoa dune field (State of Santa Catarina, Brazil), a model of eolian and pluvial activity: Internat. Symp. on the Quaternary, Boletim Paranaense de Geociencias, no. 33, p. 133-167.

CONSTRAINTS ON AEOLIAN PHENOMENA ON MARS FROM ANALYSIS OF VIKING LANDER CAMERA DATA

Arvidson, R.¹, C. Carlston,² E. Guinness,¹ K. Jones,³ D. Pidek,² C. Sagan,⁵ and S. Wall,⁴ 1. Washington University, 2. Martin Marietta Corporation, Denver, 3. Brown University, 4. NASA Langley Research Center, and 5. Cornell University.

The Viking Landers touched-down during the onset of summer in the northern hemisphere of Mars (VL1: 24° n. lat., 48° w. long., VL2: 48° n. lat., 235° w. long.). The lander cameras have been monitoring the sky and surface on a regular basis, providing information on the nature and rate of aeolian processes. As of November, 1977, monitoring has continued for three-fourths of a Martian year.

Results that impact our understanding of aeolian dynamics on Mars are:

- (1) VL1 is sitting on a wrinkle ridge, where volcanic rock outcrops are interspersed with drifts of fine-grained material (Binder, et al, 1977). VL2 may be sitting on a debris flow that is a lobe of ejecta from the crater Mie (Mutch, et al, 1977). The surface at VL2 consists of a mixture of blocks and fine-grained material. Wind-blown drifts at both sites extend from rocks and point in a southerly direction (Sagan, et al, 1977). In addition, a large drift at VL1 has accumulated in a boulder field, presumably because the boulders provided sufficient roughness to reduce wind velocities and to induce sedimentation. The southerly direction for the drifts is consistent with the direction of bright streaks seen from orbit at these latitudes and with the wind direction inferred from the Mariner 9 IR measurements near the end of the 1971 dust storm. However, Viking lander meteorology results suggest a much more complex distribution of winds. Two large "perihelion" dust storms occurred during Viking (Figure 1). Winds did not blow consistently from north to south at either site, during either storm (Ryan, personal communication).
- (2) The behavior of soils during trenching (Moore, et al, 1977), and the ability of soil material to coat lander parts, imply that much of the material is fine-grained, $\leq 100 \mu\text{m}$. Thus, the most easily moved particle size under Martian conditions, $\sim 160 \mu\text{m}$ (Greeley, et al, 1976), appears to be in a minority. Some sand-size material may occur, but mostly as aggregates of finer-grained material.
- (3) Soils exposed at both landing sites are fairly cohesive (Moore, et al, 1977), implying that threshold drag velocities (V_{*t}) needed to entrain material will be higher than for cohesionless materials. In addition there should be an upturn in the V_{*t} vs. particle size curve for small particles (Sagan, et al, 1977). However, once disturbed, the soil tends toward being cohesionless, perhaps implying that once wind initiates significant particle entrainment, the surface would be disturbed, cohesion would be reduced, and all hell would break loose.

Arvidson et al, p. 2

- (4) Viking Lander X-ray fluorescence results (Toulmin, et al, 1977) and Lander camera multispectral data (.4-1.1 μm) (Huck, et al, 1977) are consistent with the soils being composed of a mixture of weathering products derived from iron-rich igneous rocks. Similarities in composition and spectra at both landing sites imply that the soil has been homogenized by winds on a global scale. Lander camera spectra for soils are similar to spectra for bright areas seen from Earth (McCord and Westphal, 1971). The spectral characteristics of a given region on Mars probably depend on the extent of covering by bright wind-blown material and on the characteristics of in situ materials.
- (5) No obvious topographic changes have been found in comparing pictures of drifts taken on various days with the lander cameras. However, such comparisons are hampered by changes in solar elevation and azimuth with changing season. Picture differencing of a few images taken during the beginning of the mission showed no significant changes in brightness or topography (Levinthal, et al, 1977). These image pairs were typically separated by 5 to 20 Martian days. Beginning in September, 1977, pictures have been returned that have solar elevations and azimuths that are within a couple of degrees of conditions for imaging during the first fifty days of the missions. These products are ideal candidates for picture differencing to reveal subtle changes in topography and brightness over the period of half a Martian year. These data are currently being processed.
- (6) Soil located at the base of "Big Joe" at VL1 slumped sometime between the 74th and 183rd day after landing. The soil regions adjacent to the lander are cut with a series of fractures that seem to have formed by vibration during landing of the spacecraft. Most likely, the slumped zone was fractured during landing and increased V_{*t} during a mild wind gust was sufficient to initiate slumping. In addition, soil material within footpad 3, VL1, has been significantly scoured by winds. The material in the footpad is loose, and in addition, the footpad surface slopes some 30° . Thus, V_{*t} needed to entrain material will be lower than that needed to erode material on a flat surface. We estimate that the shear stress needed is some 60-70% of that needed to induce movement on a flat surface. Finally, soil material dumped onto the lander deck has been considerably shaped by wind and by the action of subsequent dumps of soil, where the soil material impacted onto older deposits and reshaped them. Unfortunately, soil deliveries and dumps have continued throughout the mission, making it very difficult to tell if wind alone has done any of the reshaping.
- (7) Reference gray patch charts mounted on the lander, and used for calibration of multispectral imagery, have obtained a coating of red dust (Bragg, 1977). Some of the dust was blown off the charts at the onset of high winds associated with the two perihelion dust storms (Figure 1). That is not too surprising since the chart surfaces slope at 79° to the horizontal, and the grains must have been held largely by adhesive forces. Consequently, the wind-

Arvidson et al, p. 3

induced shear needed to remove the dust need not be as high as that needed to erode material on a flat surface.

- (8) Lander cameras have monitored the opacity of the atmosphere through two perihelion dust storms (Pollack, et al, 1977). The first began in mid-February and the second in early June. Dust was raised largely in the southern latitudes and was then spread as a planet-wide cloud. Wind velocities at both landing sites seem to have never been high enough to erode undisturbed materials. However, an empirical comparison of the relationship between atmospheric optical depth and the distribution of surface brightness, both before and after the dust storms, shows that the surface became systematically brighter after the dust cleared from the atmosphere. The most likely explanation is that a thin dust layer, a few microns thick, was deposited onto the surface.
- (9) In sum, the past year on Mars has been a relatively quiet one in terms of aeolian activity. With the exception of some wind-induced redistribution of disturbed material, the only major change in the scene appears to be a thin coating of dust from the sky. Yet, the soil at the landing sites has, in the past, been shaped in a significant way by winds. The large drift at VLI has also been partly eroded, exposing layering both along dip and along strike (Mutch, et al, 1976).

The subsolar latitude at perihelion, the approximate location of the beginning of major dust storms, varies with time because of perihelion and spin axis precession. The subsolar latitude migrates $\pm 25^\circ$ lat. about the equator, with a period of 50,000 years (Ward, 1974). As pointed out by a number of investigators, that may mean that the dark areas, if they are regions stripped of a large fraction of the bright mobile dust layer, may also migrate about the equator with that period. If correct, that would mean that, some 20,000 years ago, most dust storms may have occurred at the latitude of VLI, and much of the soil present at the time may have been stripped away. The present deposits would then have accumulated since then, which is consistent with the southerly direction of the streaks, i.e. implying surface flow back to a more southerly subsolar latitude at perihelion. However, such a young age may not be consistent with the partially lithified and deflated nature of the drifts (Mutch, et al, 1976). Unless it can be shown that salts, which are probably the agents lithifying the soil (Toulmin, et al 1977), have cycled through the regolith at a time scale $\approx 20,000$ years, the drifts may have to be relegated to an earlier epoch in Martian history.

ORIGINAL PAGE IS
OF POOR QUALITY

Arvidson et al, p 4

Figure 1. Top graph is an averaged maximum wind velocity, courtesy B. Henry. Middle graph indicates extent of coating of the three reference gray charts with dust. A value of 1.0 indicates clean chart, while 0.0 indicates total obscuration by a dust cover. Bottom plot indicates optical depth as seen by the lander cameras. The gray patches became dirty soon after landing, probably due to sampling activities. The extent of dust cover is controlled by the maximum wind velocity - high winds blow the dust off. The surface at both landing sites seems slightly brighter after cessation of the second dust storm. Note that winds have not been high enough to cause significant entrainment at the landing sites. Rather, the increased optical depth is due to dust in the atmosphere that was entrained elsewhere and transported over the landing sites in suspension. VL2 results are similar, although complicated by the north polar hood and by the presence of ground frost.

REFERENCES CITED

- Binder, A.B., R.E. Arvidson, E.A. Guinness, K.L. Jones, E.C. Morris, T.A. Mutch, D.C. Pieri, C. Sagan, 1977. The geology of the Viking lander 1 site. *J. geophysical research*, vol. 82, pp 4439-4451.
- Bragg, S.L., 1977. Characteristics of Martian soil at Chryse Planitia as inferred by reflectance properties, magnetic properties, and dust accumulation on Viking lander 1. Master's thesis, Washington University, unpublished.
- Huck, F.O., D.J. Jobson, S.K. Park, S.D. Wall, R.E. Arvidson, W.R. Patterson, W.D. Benton, 1977. Spectrophotometric and color estimates of the Viking lander sites. *J. geophysical research*, vol. 82, pp 4401-4411.
- Levinthal, E.C., K.L. Jones, P. Fox, C. Sagan, 1977. Lander Imaging as a detector of life on Mars. *J. geophysical research*, vol. 82, pp 4468-4478.
- McCord, T.B. and J.A. Westphal, 1971. Mars: narrow-band photometry, from 0.3 to 2.5 microns, of surface regions during the 1969 apparition. *Astrophysical J.*, vol. 168, pp 141-153.
- Moore, H.J., R.E. Hutton, R.F. Scott, C.R. Spitzer, R.W. Shorthill, 1977. Surface materials of the Viking landing sites. *J. geophysical research*, vol. 82, pp 4497-4523.
- Mutch, T.A., R.E. Arvidson, A.B. Binder, E.A. Guinness, E.C. Morris, 1977. The geology of the Viking lander 2 site. *J. geophysical research*, vol. 82, pp 4452-4467.
- Mutch, T.A., R.E. Arvidson, A.B. Binder, F.O. Huck, E.C. Levinthal, S. Liebes, Jr., E.C. Morris, D. Nummedal, J.B. Pollack, C. Sagan, 1976. Fine particles on Mars. observations with the Viking 1 lander cameras. *Science*, vol. 194, pp 87-91.
- Pollack, J.B., et al, in preparation.
- Sagan, C., D. Pieri, P. Fox, R.E. Arvidson, E.A. Guinness, 1977. Particle motion on Mars inferred from the Viking lander cameras. *J. geophysical research*, vol. 82, pp 4430-4438.
- Toulmin, P. III, A.K. Baird, B.C. Clark, K. Keil, H.J. Rose, Jr., R.P. Christian, P.H. Evans, W.C. Kelliker, 1977. Geochemical and Mineralogical interpretation of the Viking inorganic chemical results. *J. geophysical research*, vol. 82, pp 4625-4634.
- Ward, W.R., 1974. Large-scale variations in the Obliquity of Mars. *Science*, vol. 181, pp 260-262.

Arvidson et al, p. 5

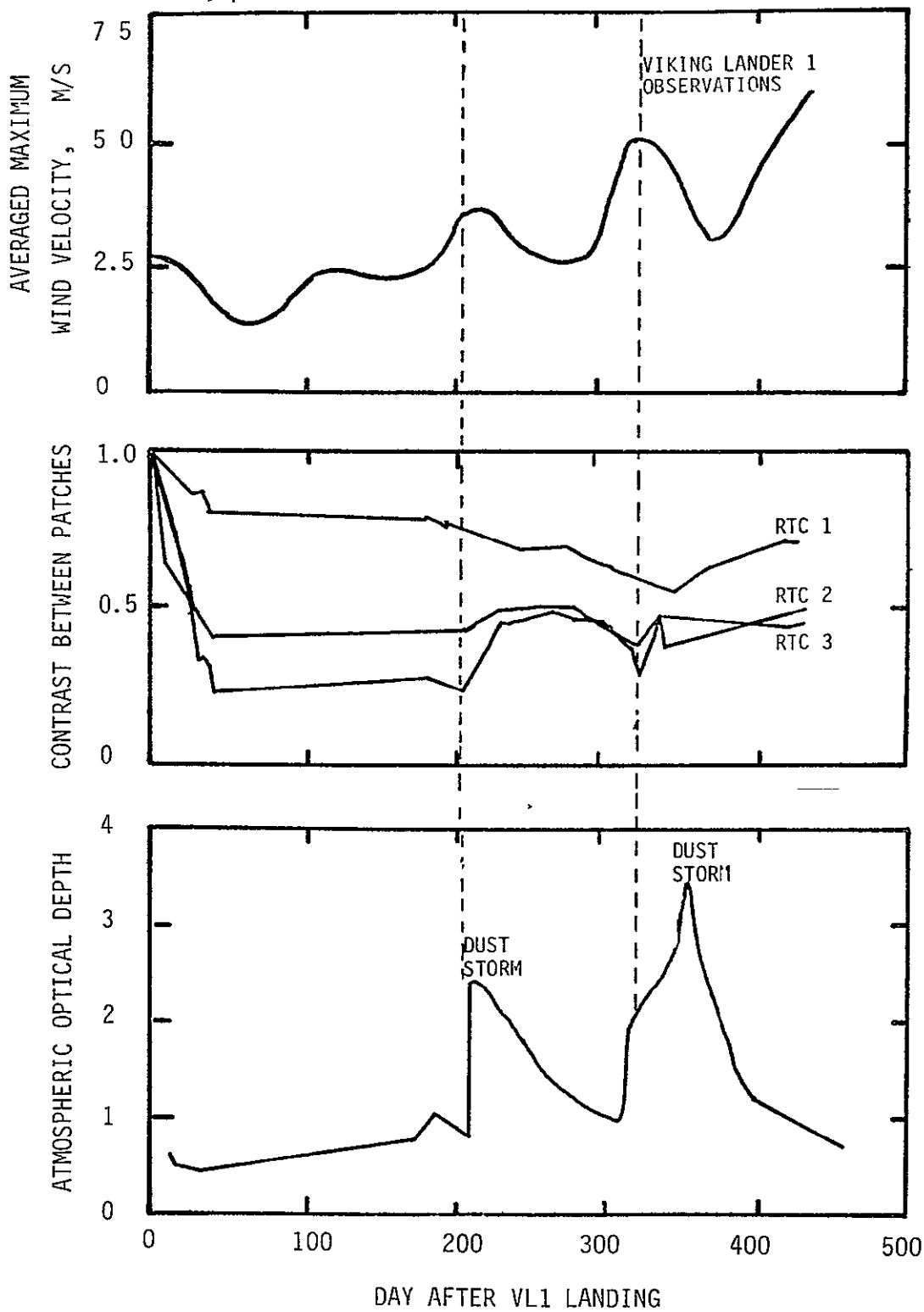


Figure 1

ORIGINAL PAGE IS OF POOR QUALITY

WIND - SAND INTERACTIONS

Bagnold R. A.

The forms of aeolean sand dunes are profoundly affected by even the sparsest vegetation. They become disorganised. Thus the effects of the free interplay of unimpeded wind and sand are most clearly seen in regions so arid as to be entirely lifeless. My interest in this process was first aroused in the late 1920's during explorations of the Egypto-Libyan desert by the high degree of organisation of the great dunes. The reason why sand collects into dunes was then a mystery as also was the physical mode of transport of the grains.

Experiment with home-made apparatus during the 1930's disclosed the mode of transport to be that of ballistic saltation. The transport rate was found by wind-tunnel measurements to be a cubic function of the wind velocity and also a function of the relative inertia of the surface grains on which the saltating grains impinge. Hence the preferential deposition of sand upon like loose sand rather than upon more rigid surfaces.

Owing to the large scale of the saltation trajectories model experiments cannot reliably imitate dune morphology. In any assumed conditions the trajectories can be computed fairly well, together with the velocity of final impact. This, on Earth, approaches the wind velocity at trajectory height. Quartz being here the only natural material capable of enduring such impacts indefinitely, the durability of dune material in Martian wind conditions needs study. It seems important to compute hypothetical Martian trajectories and to experiment on grain transport in Martian wind conditions.

The long-term global wind pattern responsible here for the strikingly common orientation pattern of all four of the great desert dune systems will be discussed, together with a postulated explanation of the remarkable straightness and parallelism of the dune chains.

The rate of sand transport being a cubic function of wind speed the direction of the annual resultant transport vector must be computed from the original meteorological records. This important vector is usually dominated by a few storm winds, so its direction may differ appreciably from that of the conventional 'prevailing wind'. The computation is quick. One year's records can be dealt with in less than two hours. Unfortunately continuous wind records are seldom if ever available for the neighbourhood of dune fields. Lack of long-term wind data severely limits the usefulness of dune studies, for dune forms are largely dependent on the local pattern of long-term variation of wind strength and direction.

DUNE TYPES AND DISTRIBUTION IN SAND SEAS, EARTH AND MARS

Breed, Carol S., U.S.G.S., Flagstaff, AZ., John F. McCauley, U.S.G.S., Flagstaff, AZ., A. Wesley Ward, University of Washington, Seattle, WA., and Steven G. Fryberger, U.S.G.S., Denver, CO.

A Landsat and SKYLAB based study of sand seas on Earth recognizes five basic dune types on the basis of planimetric shapes and slipface orientations. Dunes of these five types are widely distributed, and each type shows similar shape and pattern characteristics through a great range of sizes from simple forms, measured in meters, to compound, kilometer-sized sand mountains. The basic types are linear, crescentic, dome, parabolic, and star dunes. Numerous complex dune forms also occur, and these are comprised of various combinations of the basic types. In contrast to the global distribution of the basic dune types, however, many of the complex forms are unique to certain geographic areas.

On Earth, distribution of sand seas is in latitudinal belts, from about 30°S to about 40°N, that coincide largely with the trade winds. Some parts of the major sand seas are presently stabilized by vegetation, and these stabilized dunes are generally considered relics of more intense wind activity than the present. Fully active, very large dunes in sand seas are presently limited to desert areas that receive, on the average, no more than about 100 mm annual rainfall, or to areas where vegetation has been removed, allowing reactivation of the sand. Two or more generations of dune development can often be discerned in areas of reactivated sand, on the basis of differing types, sizes, orientations and degree of vegetative cover of the dunes observed on satellite pictures.

Association of regionally distributed dune types with specific types of regional wind regimes (unimodal, bimodal, complex) in the very large sand seas of Africa, Asia, and Australia is presently possible only in broad terms. Data obtained from sparsely distributed World Meteorological Organization (WMO) stations in and adjacent to several major sand seas are plotted as circular histograms on uncontrolled Landsat mosaics. These "sand roses" indicate the potential sand movement by all sand-moving winds greater than 12 knots from 16 compass directions throughout the year, and also show the annual resultant (net) direction of potential sand transport at each station. Though sparse, the data from the sand roses indicate a general association of certain types of wind regimes with certain basic dune types. Field studies of dune morphology in relation to local wind regimes are currently underway in the deserts of Arizona and adjacent states.

Preliminary comparisons of dunes on Earth with those discerned on Mariner 9 and Viking pictures of Mars indicate close correspondence of crescentic dune shape and dune field pattern characteristics on the two planets. The width, length, and wavelength ratios of dunes in the Hellespontus region of Mars are very close to the mean shape ratios of barchanoid dunes measured on Landsat sample areas of Earth. The distribution pattern of some dunes bounded by crater walls on Mars closely resembles the pattern of some dunes bounded by mountain fronts on Earth.

A systematic, global survey of Mars, based on Landsat and Viking pictures, has begun, in preparation for compiling a comparative catalog of desert landforms. The survey includes not only depositional features, such as

dunes, but also erosional features, such as yardangs, parallel grooves, symmetrical nubbins, and deflation pits. Regional studies of the types and distribution patterns of the Martian windforms, in comparison with similar features on Earth, will aid in the interpretation of the geological effectiveness of wind action on Mars, particularly its role through time.

STAR DUNES AS A SOLITARY FEATURE IN GRAND CANYON, ARIZONA,
AND IN A SAND SEA IN SONORA, MEXICO

Breed, William J., Museum of Northern Arizona, Flagstaff, AZ
86001 and Carol S. Breed, U.S. Geological Survey, Flag-
staff, AZ 86001

A solitary star dune lies on a beach at the bottom of Grand Canyon just south of the mouth of Fall Canyon at its junction with the Colorado River. The location is approximately River mile 211.5 below Lee's Ferry in northern Arizona. Rainfall at this locality is less than 25 cm per year.

The dune is a simple star with four arms, about 5 m high at the center and about 15 m in its longest dimension, from southwest to northeast. Observations in June, 1973, and September, 1977, illustrate changes in the growth pattern and slipface orientations of the dune (fig. 1).

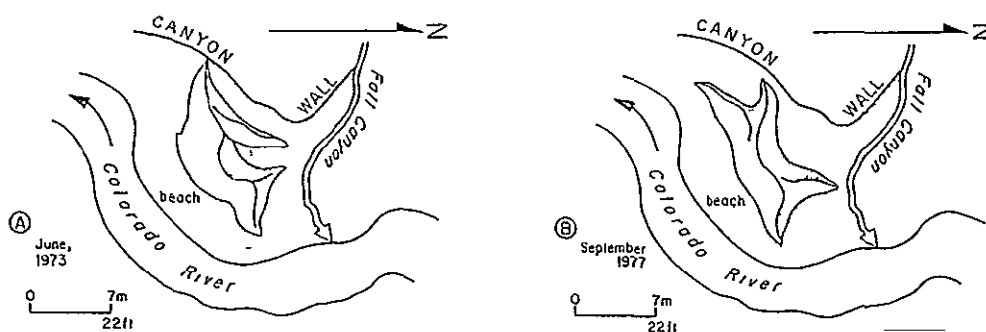


Fig.1 MORPHOLOGY OF A STAR DUNE IN GRAND CANYON, ARIZONA

At both times of observation, the dune was dominated by large, north-facing avalanche slopes. These are interpreted as resulting from the strong prevailing winds that blow up canyon from the south. Extension of two dune arms southward, observed in 1977, is interpreted as resulting from reversal of sand transport direction due to occasional strong down canyon winds that blow from the north. A third direction of sand transport is believed necessary to produce star dunes instead of reversing dunes. The third direction, in this case, is provided by west winds that sweep down Fall Canyon.

The net effect of the three wind directions is to produce a dune with multiple arms, each steep-sided due to repeated reversals, and to prevent migration of the dune northward into the side canyon or southward into the Colorado River, where it would be destroyed by running water.

ORIGINAL PAGE IS
OF POOR QUALITY

The precarious existence of the star dune in Grand Canyon is possible only because of the entrance of Fall Canyon from the west, into an unusual stretch of the Colorado River that runs north-south, parallel to two strong winds. The entrance of Fall Canyon provides both a source of sand which is renewed periodically by floods, and a corridor for the third wind, from the west. East winds are rare in this region, which may explain the lack of star dunes along other, generally east-west, stretches of the river.

In contrast to the solitary star dune in Grand Canyon, great fields of star dunes, some more than 150 m high, have formed in the Gran Desierto of Sonora, Mexico. The star dunes are distributed across a 1500 km² sand sea. In the center of this sand sea are huge, compound star dunes that range up to 1.2 km in diameter. Most are aligned in parallel rows that trend N 55°W, but around a topographic barrier known as the Sierra del Rosario, the dunes seem to be distributed at random.

Wind processes that build fields comprised of myriads of star dunes are not well known. Arms of the star dunes are characteristically steepened on both sides indicating repeated reversals of sand transport direction by opposing winds of nearly equal strengths. Winds measured at Punta Penasco, Mexico, suggest seasonal changes of the resultant directions in the Gran Desierto, from ESE in winter to NNE in summer. Studies of the distribution of grain sizes in the star dunes are expected to help delineate the patterns of wind transport that produced them.

AEOLIAN STRIPPING OF ASH LAYERS IN THE KAU DESERT, KILAUEA VOLCANO,
HAWAII

Dzurison, D., Hawaiian Volcano Observatory, Hawaii Volcanoes National
Park, HI 96718

Preliminary field investigations indicate that aeolian stripping has played a significant role in landscape evolution in the Kau Desert region south of Kilauea caldera on the island of Hawaii. Remnants of an extensive deposit of relatively fine grained volcanic ash are exposed at the surface roughly 10 km south of the Kilauea summit. Contacts with underlying pahoehoe flows to the north are generally sharp, and are locally expressed as a single, near vertical scarp as much as 50 cm high. In plan view, the contact is seen to consist of several lobes which point northeastward, into the prevailing trade winds. Dune forms aligned along the contact have been at least partially stabilized by enhanced shrub and tree growth at the ash/pahoehoe boundary.

If the Kilauea summit region was the source area for this ash deposit, then a minimum of $5 \times 10^7 \text{ m}^3$ have been removed from the area immediately south of the caldera. No adequate sink for this volume of material has yet been identified on land, suggesting that much of it has been transported to the sea, 15 km south of Kilauea caldera. Effective transport of large volumes of volcanic ash by winds, and the resulting distinctive surface morphology created by relatively uniform scarp retreat combine to make the Kau Desert an attractive field area for analog studies of aeolian processes on Mars, where stripping is generally acknowledged to have been an effective erosional agent.

Additional field work in progress is intended to further quantify the volume of eroded ash, evaluate the stability of the present ash distribution, and explore implications of massive stripping for the perceived eruptive history of Kilauea.

ORIGINAL PAGE IS
OF POOR QUALITY

EXPERIMENTAL EOLIAN EROSION BY VERY FINE GRAINS AT TERRESTRIAL AND MARTIAN ATMOSPHERIC PRESSURES

Forsman, N.F., University of Houston, Houston, TX 77004

Laboratory tests have involved the examination of textural modification of both projectiles and obstacles subjected to a simulated eolian impact environment. Natural obsidian obstacles were placed on the floor of a small "race track" air tunnel and impacted independently by groups of crushed, 74-88 micron grains of quartz, magnetite, orthoclase, augite, and olivine. Experiment run times of two, twenty, and fifty hours were used with an air speed and pressure of 15 meters per second and 14.78 lb/in², respectively. A series of comparative tests were conducted with augite at much reduced atmospheric pressures to address the question of how mechanics of eolian erosion on Mars may be affected by its low atmospheric pressure.

Results indicate that proposed lower size limits (Kuenen, 1960) of grains capable of acting as agents of eolian erosion or themselves showing textural modification as a result of eolian abrasion are invalid. Grains of extremely small size are potential tools of eolian erosion even on Earth. Previously suggested atmospheric "cushioning" influences are real, but do not produce an absolute minimum size limit for grains capable of eroding. Instead, they effect a decrease in rate of erosion of materials. The difference in atmospheric cushioning between terrestrial and Martian atmospheric pressure conditions is great. A subjective estimation places at least an order of magnitude difference in eolian erosion rate for terrestrial and Martian conditions if only differences in atmospheric cushioning influences are considered.

Once grains are lifted from the Martian surface by the drag force exerted by threshold wind conditions, they travel along either in saltation or suspension modes, depending on their size and the actual wind velocity. While actually above the surface, these grains will travel at velocities roughly equivalent to wind velocities. This, plus the reduced atmospheric cushioning influences on Mars, enables even extremely fine grains, once in motion, to act as very capable instruments of erosion. A person standing on Mars in a 300 mile per hour wind may scarcely feel the movement of such a diffuse fluid past him, but would feel the full force of small grains impacting against his body at close to these same wind velocities.

Whether grains are transported by the winds of Mars in saltation or suspension modes is largely irrelevant to questions concerned with the abilities of these grains to effect erosion of obstacles in their paths. Even grains of such small size as to be generally carried in suspension are capable agents of erosion, with their erosive strength being determined primarily by their mass and velocity. Dietrich (1976) has provided evidence from experimentation indicating that erosion is not even dependent upon differences in mechanical strengths of projectile and target. Rather, sufficient energies supplied by the moving projectile to break molecular bonds in the target structure are required. Due to the high velocity component of equations of kinetic energy of impact for particles carried by Martian winds, even projectiles of very low mass can and probably do serve to erode the surface of that planet. Martian dust storms probably are quite effective

in eroding even surfaces that stand above reasonable saltation heights.

REFERENCES CITED

Dietrich, R.V., 1976, Impact Abrasion of Harder by Softer Materials:
J. Geol., V. 85, pp 242-246.

Kuenen, Ph.H., 1960, Experimental Abrasion 4: Eolian Action: J. Geol.,
V. 68, pp 427-449

TECHNIQUES FOR THE STUDY OF EOLIAN SAND SEAS

Fryberger, Steven G., and Ahlbrandt, Thomas S., U.S. Geological Survey, Denver, CO 80225.

An important method of study of large sand seas is to assemble mosaics of Landsat imagery (scale 1:1,000,000) of the world's largest dune tracts (noting dune types and their distribution) and to evaluate surface wind summaries for the same regions, in terms of potential sand movement. In order to evaluate potential sand movement, a weighting equation is required because rate of sand movement is an exponential function of wind velocity.

To make estimates of relative sand movement, weighting factors are derived from the arithmetic means of velocity groups in standard wind summaries and are then multiplied by a time factor (% in the wind summary) and totalled. The resulting numbers, known as drift potentials (DP), are proportional to the amount of sand drift during the time period considered. Drift potentials can be evaluated in terms of direction and be resolved trigonometrically to a resultant drift potential (RDP), and a resultant drift direction (RDD). The ratio of RDP/DP constitutes an index of the directional variability of effective wind. The directional components of drift potential can be plotted in a circular histogram, with arms pointing "upwind," known as a sand rose. Use of the technique described above has resulted in the following (a) recognition of fundamental differences in wind energy in the world's major deserts, (b) recognition of five distinctive effective wind regimes, as revealed by sand roses, associated with certain dune forms, and (c) additional evidence for the potential long range drift of sand by wind.

Modern sand seas have widely differing amounts of wind energy. The windiest deserts, in which sand movement is probably greatest, are the An Nefud of Saudi Arabia and the deserts of Northwestern Libya and Mauritania. Arabia and Mauritania are characterized by strong anticyclonic (high pressure) circulation which peaks in energy when anticyclonicity is at a maximum, or the zone between the semi-permanent high and low pressure systems has the highest pressure gradient. The least windy deserts, such as the Taklamakan of China and the Kalahari of South Africa lie near the center of semi-permanent high pressure cells. Some desert regions such as Western Mauritania are strongly zoned, in terms of wind energy.

Five common patterns of effective wind regimes, as expressed in sand roses, occur frequently in the deserts studied. These effective wind regimes are classified by arrangements of modes (groupings of arms) on the sand roses as follows: (a) narrow unimodal--single mode with 90% of the drift potential in two adjacent directional categories; (b) wide unimodal--any other distribution with a single peak or mode; (c) acute bimodal--two modes meeting at an angle less than or equal to 90°; (d) obtuse bimodal--any other bimodal distribution; (e) complex--more than two modes. Simple effective wind regimes, such as unimodal and bimodal are often associated with strong coastal (trade) winds and anticyclonic circulation. Complex wind regimes are often associated with cyclonicity and the winds of several directions associated with frontal passages and following winds. Barchanoid dunes are common in unimodal wind regimes, linear dunes in wide unimodal, and bimodal wind regimes and star dunes in complex wind regimes.

The possibility of long range sand migration in some deserts suggested by some earlier workers is strongly supported by information obtained from present methods. Evidence from Landsat imagery includes: (a) extended rectangular or broadly curving shapes of sand seas in Mauritania, Saudi Arabia and elsewhere, aligned with the direction of effective winds; (b) sand streaks and "shadows" extending hundreds of kilometers in Saudi Arabia and Libya, aligned with the effective wind; (c) occurrence of large sand bodies in areas where it is unlikely that sand was brought in by fluvial agencies (e.g. Mauritania), (d) transgression of high relief topography (including drainages) by sand streaks and dunes in high wind energy areas such as Upington, South Africa, indicating that at least locally the power of the wind to move sand exceeds that of water in the drainages; (e) absence of sand accumulation near mouths of some major wadi systems in Algeria where accumulation might be expected. Instead, in this high energy region, only streaks are observed parallel to the effective wind, with the nearest large sand body over a hundred miles away. Calculations based on improved quality surface wind data indicate annual values of sand movement of greater than $30M^3/M/YR$ in regions of greater than 400 V.U. total drift potential.

In addition to quantitative techniques of analysis of wind records and space imagery, improved ground-based methods of study of sand sea dynamics have been developed. These methods include principally the use of sand trapping devices for the measurement of instantaneous, or long term rate of drift of sand across the surface of a desert.

Instantaneous rate of sand drift as a function of wind velocity can be measured using a directionally responsive, vertical type sand trap. This trap is 1.5 m high, with a 1 cm width vertical aperture. Sand enters the aperture and falls into a container within a base buried below the sand surface. The container rests on a pressure transducer which transmits a signal along a buried cable to a digital readout up to 60 m distant. Use of this device allows accurate, instantaneous measurement of rate of sand drift for 15-30 minutes during conditions in which rates of drift average about .25-.50 g/cm/sec.

Longer period observations of rate of sand migration are possible with a different trap type, distinguished principally by a smaller aperture (.25 cm) and larger storage volume for collected sand. The sand is stored in separate compartments oriented in specific directions; direction of sand drift as well as total amount are thus accurately recorded.

ORIGINAL PAGE IS
OF POOR QUALITY

TESTS OF A PORTABLE WIND TUNNEL FOR DETERMINING WIND EROSION
THRESHOLD VELOCITIES

Gillette, D. G., National Center for Atmospheric Research,
Boulder, Colorado 80307.

A portable wind tunnel having a floor formed by a small flat expanse of natural soil may be used to create artificial turbulent winds to test for soil threshold velocity. Three soils were tested, ranging from a pebble covered desert soil to a relatively sandy agricultural soil. Threshold velocities for the three soils showed the importance of the size distribution of the surface material. The larger proportion of mass in particles or aggregates which were nonerodible rendered the material increasingly nonerodible. Thus larger threshold velocities were required to initiate wind erosion.

GEOLOGY AND AEOLIAN FEATURES OF THE HELLAS BASIN FLOOR

Greeley, R., P. Spudis, and D. Johannesen, Dept. of Geology and Center for Meteorite Studies, Arizona State University, Tempe, AZ 85281

Viking Orbiter 1 has provided the first contiguous photographic coverage of the floor of the Hellas basin and although atmospheric haze appears to obscure the region around the main basin rim, medium resolution images (250 m per pixel) have revealed surface detail. The Hellas basin floor was first photographed by Mariners 6 and 7 in 1969; the term "featureless terrain" was applied to the floor as no surface detail was visible (Sharp and others, 1971). Mariner 9 arrived at Mars in 1971, during a global dust storm, that obscured the planet. Hellas was one of the last areas to clear after the storm, however, even after it had cleared, the floor materials remained "featureless" and the impression was gained that Hellas was an enormous "dust bowl". Only very late in the Mariner 9 extended mission did a single "B" frame show any surface detail (Mutch and others, 1976). This study, based on Viking Orbiter images, was undertaken to provide the first systematic mapping of the major regions of aeolian activity in the Hellas basin. The Hellas basin is an extremely old, degraded multiringed impact basin approximately 2000 km in diameter and more than 7 km deep in some areas (Wilhelms, 1973). The shallow depth of the basin argues for extensive postbasin infilling and the presence of wrinkle ridges is suggestive of volcanic flooding. The lack of lunar Archimedes-type craters as well as a notable lack of small volcanic landforms suggests these lavas were rapidly emplaced soon after basin formation as "flood volcanics" (Spudis and Greeley, 1977). Several sinuous channels appear to "empty" into the basin, possibly indicating fluvial activity (Potter, 1976). The "featureless" nature of basin floor materials as seen in previous photography has been taken as indicating great accumulations of aeolian sediments, possibly hundreds of meters thick (Scott, and Carr, 1977).

Viking photos have revealed many positive relief landforms on the basin floor as well as numerous albedo markings attributed to the effects of aeolian erosion and deposition (Sagan and others, 1972, 1973). Relatively straight to weakly sinuous ridge-like structures interpreted as dunes occur in several areas in Hellas (fig. 1). The dune-like features averaging 3 to 5 km in length and are on the order of 1 km in width. Typically they are clustered in groups that display no obvious correlation with regional topography. Mapping of inferred wind directions by dark streak orientations confirm earlier conclusions of a dominant east to west wind direction (Veverka and others, 1977) and show that long axes of the dunes of various fields are oriented both parallel and perpendicular to prevailing wind directions. This is interpreted as indicating the probable presence of longitudinal dunes (such as Dune Field 1) having long axes aligned parallel to wind direction and transverse dunes (Dune Field 8) with long axes aligned perpendicular to prevailing wind directions. Almost all dune fields lie within the relatively flat portion of the basin floor except Dune Field 4 which occurs on a regional east-west slope, these dunes may be migrating upslope. In addition, several smaller clusters of dunes (unmapped) were noted in crater floors on the western rim of the basin. One of the more enigmatic landforms of the basin are clusters of equant positive relief features, 5 to

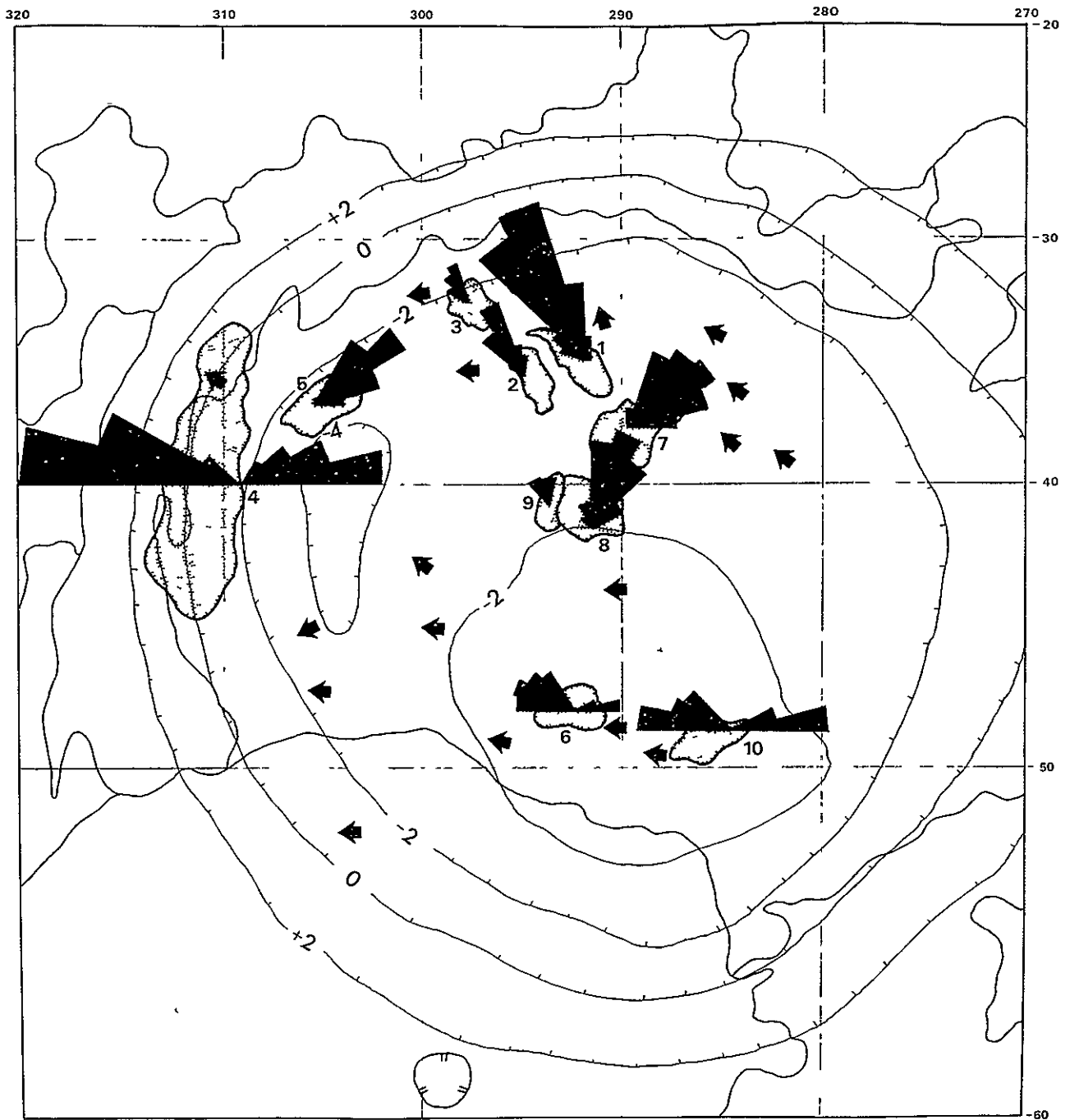


Figure 1. Azimuth-frequency diagrams of the orientation of the long axis of dunes in the major dune fields (stippled-numbered) of the Hellas basin. Arrows indicate inferred wind directions based on orientation of dark streaks. Contour interval is 2 km.

10 km in maximum dimension. These features may represent fields of equant dune or deflation landforms (yardangs) produced by shifting directions of aeolian erosion.

Summary and Conclusions

The geology of the Hellas basin floor is much more complex than previously considered. The large multiringed impact basin probably was filled extensively by flood volcanics soon after its formation. The floor of the basin is not a featureless plain, but appears to consist of a complex series of interbedded volcanic flows, aeolian deposits, and possibly fluvial sediments. Higher resolution coverage of the extensive dune fields and erosional landforms are desirable targets for photography during the Viking extended mission.

REFERENCES CITED

- Breed, C.S. , 1977 Terrestrial analogs of the Hellespontus dunes, Mars. Icarus, V. 30, pp. 326-340
- Cutts, J.A. and Smith, R.S.U. , 1973 Eolian deposits and dunes on Mars. Jour. Geophys. Res., V 78, pp. 4084-4095
- Cutts, J.A. and others, 1976. North polar region of Mars Imaging results from Viking 2. Science, V. 194, pp. 1329-1337
- Mutch, T.A. and others, 1976 The Geology of Mars Princeton Univ. Press, Princeton, N.J., 400 p
- Potter, D.B., 1976. Geologic map of the Hellas quadrangle of Mars. U.S. Geol. Survey Misc. Geol. Inv. Map I-941.
- Sagan, C. and others, 1972 Variable features on Mars Preliminary Mariner 9 results. Icarus, V. 17, pp. 346-372.
- Sagan, C. and others, 1973 Variable features on Mars, 2, Mariner 9 global results. Jour. Geophys. Res. V. 78, pp. 4163-4169
- Scott, D.H. and Carr, M.H. , 1977. Geologic map of Mars. U.S. Geol. Survey Misc. Geol. Inv. Map (in press).
- Sharp, R. P., and others, 1971. The surface of Mars 2. Un cratered terrains Jour. Geophys. Res, V 76, pp. 331-342
- Spudis, P. and Greeley, R., 1977. Volcanism in cratered uplands of Mars: A preliminary Viking view. EOS, V. 58, p. 1182.
- Veverka, J. and others, 1977. A study of variable features on Mars during the Viking primary mission. Jour. Geophys. Res. V 82, pp. 4167-4187.
- Wilhelms, D.E. , 1973 Comparison of martian and lunar multiringed circular basins Jour. Geophys. Res. V. 78, pp. 4084-4095

ORIGINAL PAGE IS
OF POOR QUALITY

THE NUBIAN DESERT: A PRODUCT OF QUATERNARY CLIMATIC CYCLES

Haynes, C. V., The University of Arizona, Tucson 85721

The Nubian Desert, as dry as any place on Earth, is today an eolian derived landscape with no integrated drainage systems. The only vestige of former rivers are a few sinuous ridges of wind-resistant channel gravels (inverted wadies) most common near the Nile, and small dry stream beds at the base of the higher escarpments. The entire landscape consists of nearly flat plains separated by escarpments and relieved by erosion remnants (inselbergs) without significant pediments, and deflational hollows created by differential erosion by wind on a grand scale.

Overriding the bedrock landforms are the eolian deposits of the Libyan Desert studied by Bagnold and others. From satellite photography the alignments of these mobile forms with prevailing wind directions of northeast Africa is outstanding. The sands are the bedload of a colossal braided airstream with major anabranches going around the Gif Kebar - Jebel Uweinat highlands. To the north lies the Great Sand Sea with undulating mountains of sand (whalebacks) fingering out southward into parallel longitudinal (sief) dunes beyond which elongate clusters of barchands are aligned along the same arcuate streamlines. The center of the Nubian Desert, an incredibly flat area of some 100,000 sq. km. broken only by a few hills and scarps, is a slightly depressed area covered by smooth sand sheets.

The geochronology of these features and the rates of processes involved are being ascertained by investigations at stratified archaeological sites which reveal at least four major pluvials separated by periods of complete desiccation and intense eolian activity during the Late Quaternary. Deposits of the Neolithic pluvial, 7000 to 4000 B.C., consist of beaches and playa sediments, commonly as clusters of yardangs in deflational hollows, and are the best preserved of the pluvial deposits. From this evidence we can extrapolate back to Mousterian and earlier pluvials and assume that the fluctuations were of comparable if not greater magnitude. Herein must lie the main cause of erosion of the Nubian Desert in Pleistocene time. Disagreement as to whether the landforms derive from wind action or water are both in part valid in that they represent the dominant processes in two parts of a cycle in which one climatic regime prepares the land for reworking by the other. Thus pluvial episodes promote 1) weathering which weakens exposures of bedrock, 2) drainages that dissect the land, 3) lakes that fluctuate and evaporate, and 4) vegetated soils which support life in relative abundance. The intense eolian activity of the hyper-arid intervals strips away the mantles weakened by weathering, erases drainages, deflates the sediments expanded by efflorescence, and reactivates dunes which provide the abrasives for sandblasting. Under one regime life like that of the semi-arid region to the south flourishes, under the other life is denied to all but the most adapted creatures.

Remnants of relict terra rossa soil in solution cavities on the Egyptian Plateau indicate the surface to be the remnant of an early or pre-Pleistocene karst terrain that may correlate with the relict red soils of

central Sudan which appear in Gemini II photographs to be truncated by the deflational surface of the Libyan Desert. The resistance of the Gifl Kebir Plateau to wind erosion may be due to feruginization and silicification from ground water heated by basaltic intrusions. Wadies in the Gifl are without catchments, the explanation of which is unsettled. A new hypothesis is offered suggesting that former drainage basins were in shales that once overlaid the plateau but that have since been eradicated by wind.

COMPARISON OF WIND-TUNNEL-MODEL AND ATMOSPHERIC FULL-SCALE EXPERIMENTS OF
THE AMBOY CRATER AND ADJACENT TOPOGRAPHY

Abstract

Iversen, J. D., Iowa State University, Ames, Iowa 50011 and Ronald Greeley, Arizona State University, Tempe, Arizona 85281.

Mariner 9 and Viking Orbiter spacecraft photographs show streaks associated with raised-rim craters which are caused by strong surface winds. A very similar dark streak associated with a volcanic crater (cinder cone) exists in the Mojave Desert (near Amboy, California). The contrasting surface albedos are caused by light-colored sand lying over a prehistoric dark-colored lava flow. The cinder cone is essentially a truncated cone 500m in diameter at the base, 240m at the top and 75m high. The surrounding lava flow constitutes a rough but relatively uniform surface.

Three 15m meteorological towers were erected at the Amboy crater site. One was placed 3300m upstream of the crater center in a relatively smooth-surfaced alluvial fan. The second was placed 400m upstream (but displaced laterally) in the middle of the relatively rough surfaced lava flow and the third tower was placed 600m downwind of the crater center. Of the 330 time periods for which data were taken over a 2-month period (Jan-Feb. 1976), 35 time-period runs were selected for final data reduction for which strong unidirectional winds were blowing from the northwest (streak direction).

Because the relative heights of the anemometers above the mean surface of the uneven terrain surrounding each tower are unknown, the wind velocity logarithmic profile is written including a zero-plane displacement height D as follows:

$$u = (u_* / 0.4) \ln ((z+D)/z_0)$$

It is assumed in writing this equation, for the strong winds for which data were taken, that the atmosphere is neutral or very near neutral. The composite results for the 35 runs for strong northwest winds are listed in Table I.

TABLE I Wind Speed Profile Data - Northwest Wind

| <u>Tower Number</u> | <u>z_0 (m)</u> | <u>D (m)</u> | <u>$u_* / U@ 15.24$ m</u> | <u>Number of runs</u> |
|---------------------|-----------------------------|---------------------------|--------------------------------------|-----------------------|
| 1 | 0.0017 | -0.113 | 0.044 | 15 |
| 2 | 0.0085 | 0.436 | 0.053 | 16 |
| 3 | 0.101 | 0 | 0.080 | 4 |

The average ratios of friction speed between towers for data taken simultaneously are $u_{*2} / u_{*1} = 1.2$ and $u_{*3} / u_{*1} = 2.1$. The rougher surface in the lava flow (Tower 2) resulted in a considerably larger roughness height and about a 20% larger surface friction speed than in the smooth alluvial fan (Tower 1). The highest wind speeds and surface friction speeds, however, were recorded on Tower 3, located in the crater wake streak.

ORIGINAL PAGE IS
OF POOR QUALITY

In order to investigate in more detail the flow patterns near the crater a 1/1000 scale model of the crater area (representing an area 1200 x 3650m) was placed in the atmospheric boundary layer wind tunnel. The total fetch modeled in the wind tunnel upwind of the windward crater rim was 4500m (4.5m in the tunnel) for a fetch-length Reynolds number of $9(10)^6$. The wind tunnel model turned out to be slightly rougher aerodynamically than the full scale topography (u_x/U at 15.24m at Tower 2 was 0.062, 16% higher than Tower 2 in the atmosphere) In addition to the Tower 2 and Tower 3 profile data, which compare well with the atmosphere, wind speed profiles were obtained at forty-two additional locations near the crater. The wind tunnel and atmospheric velocity profiles are shown in Figs. 1 and 2.

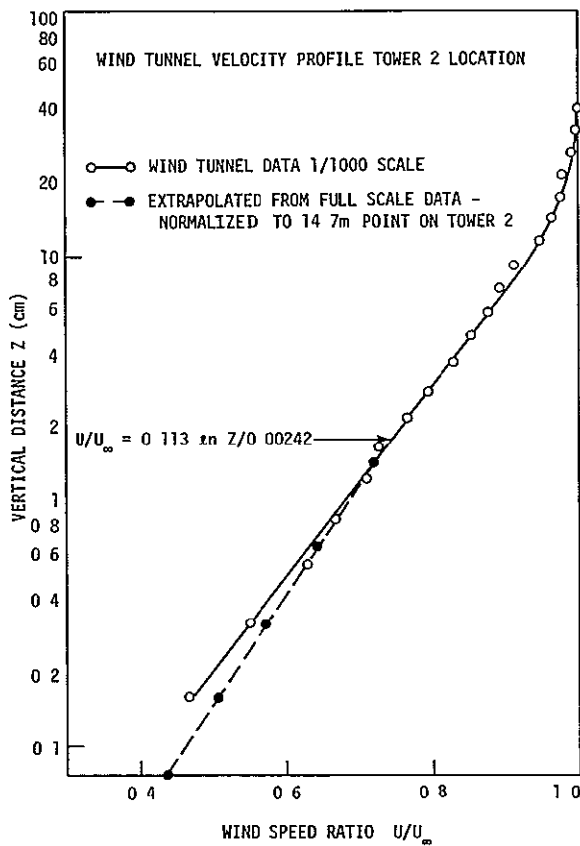


Fig. 1. Wind Tunnel - Field
Data Comparison - Tower 2

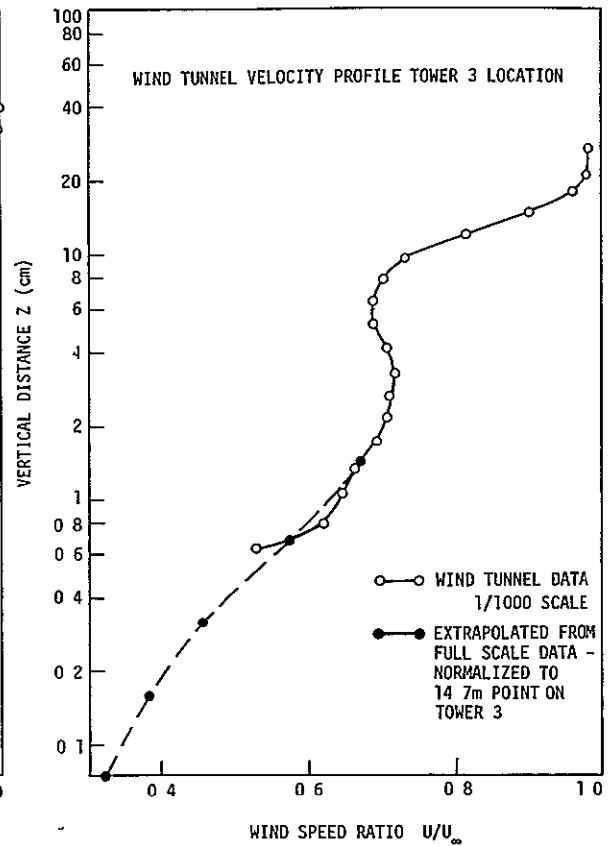


Fig. 2. Wind Tunnel - Field
Data Comparison - Tower 3

The wake streak characteristics are interpreted and explained with the aid of the wind tunnel velocity data, and also with the aid of additional experiments involving the movement of saltating material (glass spheres) over the model surface. Additional interesting wind caused albedo features of the Amboy lava flow are presented.

ORIGINAL PAGE IS
OF POOR QUALITY

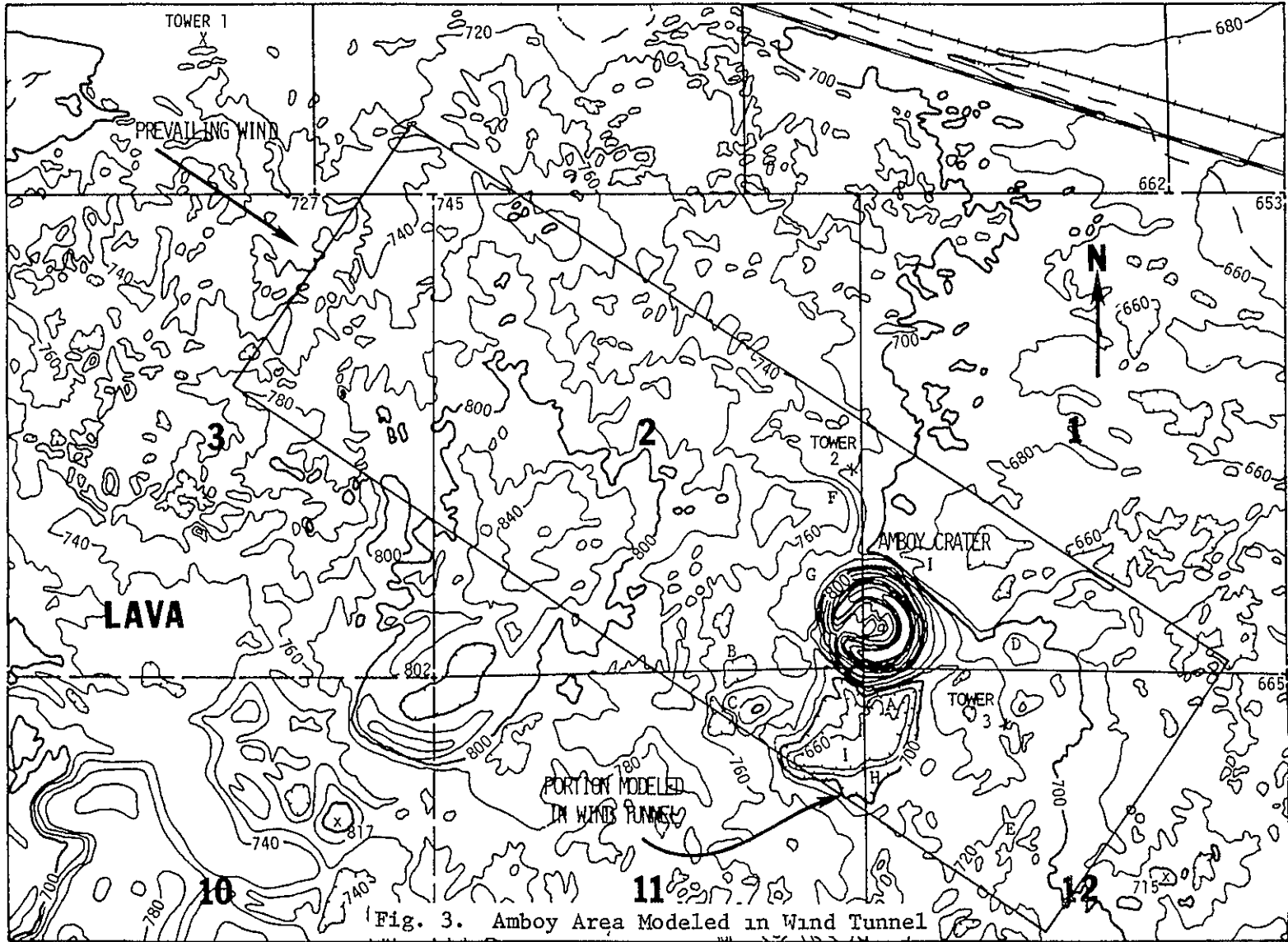


Fig. 3. Amboy Area Modeled in Wind Tunnel

ORIGINAL PAGE IS
OF POOR QUALITY

MARTIAN SURFACE PARTICAL SIZES DETERMINED BY THERMAL MAPPING

Kieffer, Hugh H., Department of Earth and Space Science,
 University of California, Los Angeles, CA 90024; and
 Frank Don Palluconi, Jet Propulsion Laboratory, California
 Institute of Technology, Pasadena, CA 91103

The thermal conductivity of dry particulate material is strongly dependant upon the particle size; this basic relation enables remote observations of temperature to be used to estimate surface material properties and map their variation. The thermal inertia, $I = \sqrt{K\rho C}$ (here in units of $0.001 \text{ cal/cm}^2 \text{ sec}^{1/2} \text{ K}$), is an important intermediate parameter in this process as it can be related both to the variation of the temperatures observed and to physical models of the surface. Using the Viking IRTM, the thermal inertia has been mapped over much of the equatorial region of Mars and, if interpreted in terms of a homogenous material, corresponds to a particle size range which would be susceptible to transport by the martian atmosphere.

A survey of laboratory observations (Kieffer et al., 1973) showed that under martian surface conditions the thermal conductivity, K , was roughly linear with the mean particle size in the range from 50 to 500 μm and varies approximately as the square root of the gas pressure. The specific heat, C , does not vary greatly amongst geologic materials, and a density, ρ , of 1.7 g cm^{-3} is assumed here in relating thermal inertia to effective particle diameter through thermal conductivity.

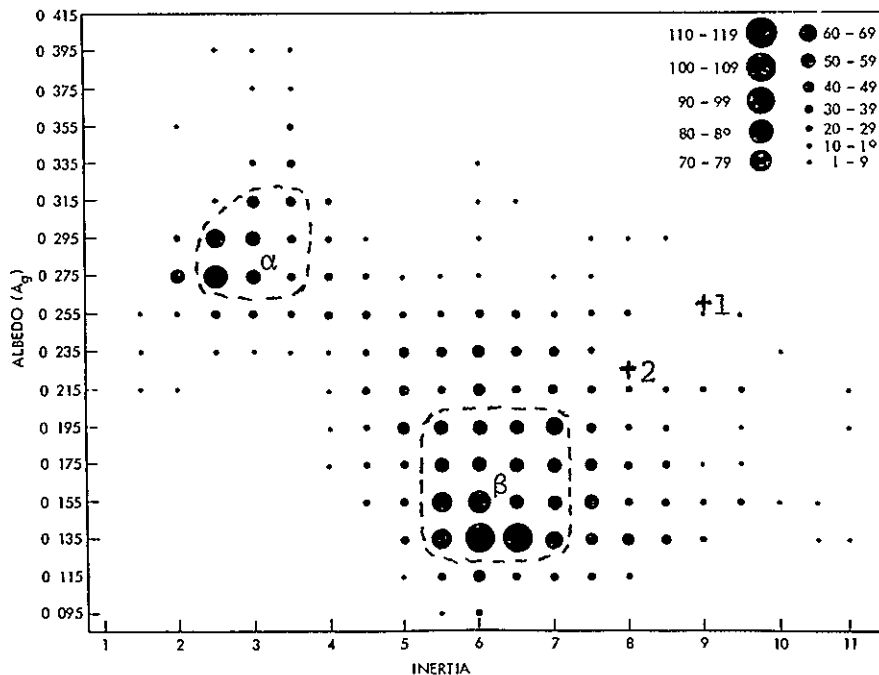
The inertia-albedo relationship for the equatorial survey is shown in the figure (see Kieffer et al, 1977, for details of this survey). There are two major populations; a fine-grained bright material, termed α , and a more abundant coarse, darker material termed β . The boundaries of the α material, $I=2.2$ to 3.7 , correspond to an effective grain diameter range of 25 to 80 μm ; the inertia boundaries shown for the β material, $I=5.2$ to 7.7 , correspond to diameters of 175 to 500 μm . In the area surveyed, 16 and 55% of the martian surface are covered by material in these two size ranges, respectively. That the distribution is distinctly bimodal suggests that the two putative surface components have differing mineral or chemical composition, rather than representing simply two size fractions of the same material. The samples intermediate between the two major populations probably represent mixtures of the two materials below the resolution of this survey (120 km), and the brighter samples at the inertias of the two major populations probably represent the occurrence of clouds effecting the albedo determination of a small fraction of the samples.

The thermal inertia and albedo of the Viking Lander sites 1 and 2 were 9-0.26 and 8-0.225 respectively (Kieffer, 1977) and are indicated in the figure. Lander imaging at these two sites indicates that the surface has a block population which would

increase its apparent inertia above that of the fine-grained material there. Comparison of the landing sites with the thermal mapping survey indicates that they certainly are not representative of either of the two common surface types.

The pervasive covering of the martian surface by fine-grained material, and the corresponding rarity or absence of regions with large areal fractions of exposed bedrock (which would have inertia of 30 or more) may result in part from the absence of a fluvial system sink (eg. deep oceans) for the fine-grained products of aeolian erosion. Since grain bonding, the presence of rocks, or atmospheric opacity all increase the apparent inertia of the surface, the effective grain diameters related to these inertias are upper limits on the size of the fine-grained component of the martian surface. That the propodderance of the martian surface is composed of material of diameter less than 500 μm indicates that the majority of the martian surface seen by remote sensing has been transported or moved by the atmosphere.

The current martian surface has likely been sorted by a wind regime which moves the α material more frequently than the β material. Some support of this is offered by the common occurrence of craters whose interior floors have higher inertia (coarser material) than the surrounding intercrater plains. We speculate that these craters are regions where the β material is selectively trapped or that the α material is readily removed.



REFERENCES CITED

- Kieffer, H.H., 1976. Soil and surface temperatures at the Viking landing sites. *Science*, vol. 194, pp 1344-1346.
- Kieffer, H.H., S.C. Chase Jr., E. Miner, G. Munch and G. Neugebauer, 1973. Preliminary report on the infrared radiometric measurements from the Mariner 9 spacecraft. *Jour. Geophysical Research*, vol. 78, pp 4291-4312.
- Kieffer, H.H., T.Z. Martin, A.R. Peterfreund, B.M. Jakosky, E.D. Miner and F.D. Palluconi, 1977. Thermal and Albedo mapping of Mars during the Viking primary mission. *Jour. Geophysical Research*, vol. 82, pp 4249-4291.

SURFACE TEXTURES OF SAND SIZED PARTICLES ABRADED UNDER EARTH AND MARTIAN CONDITIONS

Krinsley, D H and Greeley, R *, Dept of Geology, Arizona State University, Tempe, AZ 85281, *and NASA Ames Research Center, Mail Stop 245-5, Moffett Field, CA 94035

Although very little is known concerning rates of aeolian erosion on the planet Mars as compared to those on Earth, very high velocity winds and low atmospheric pressures probably have considerable effect both on erosion rates and landforms created thereby. This problem has been studied by using techniques developed to analyze quartz sand surface textures

Earth and martian aeolian abrasion of crushed quartz was simulated in wind tunnels and a laboratory erosion device at pressures corresponding to those on the two planets, the surface textures of the abraded materials were studied via scanning electron microscopy. Differences in aeolian abrasion on the two planets were indicated by differences in surface texture or roughness. Quartz was used as experimental material because a great deal of information is available on its surface characteristics, in particular, mechanical aeolian action on Earth has been studied in detail and a number of specific surface textures at various sand and silt sizes characteristic of large, hot deserts have been delineated (Krinsley et al., 1976). Subsequently, the same procedure will be followed using basalt rather than quartz, since the surface and sediments of Mars likely include a great deal of the former material.

Laboratory Experiments

Samples of crushed Brazilian quartz (175-355 and 500-850 μ m) were examined and photographed with the scanning electron microscope. The samples were then abraded with particles at 8 meters per second under Earth (740mm Hg) and martian (3mm Hg) pressures for periods of 20 minutes, one hour, three hours, four hours, and eight hours.

Fresh crushed Brazilian quartz contains a series of irregular fracture surfaces which are generally similar at grain diameters from 1 to 500 μ m, grains are angular. During simulated mechanical (aeolian) abrasion at both high and low atmospheric pressures, mechanical action starts on grain edges and with time works its way over entire surfaces, thus rounding the grains. The textures produced are very similar to those found on quartz grains from hot deserts (Krinsley et al, 1976). However, under low atmospheric pressures the process appears to operate more rapidly even though impact velocities were the same, thus grains of the same size run at low atmospheric pressures are more abraded than those at high pressures.

The following textural differences between abrasion at low and high atmospheric pressures were noted

- 1) Upturned cleavage plates are broken irregularly to a greater extent at low than high atmospheric pressures
- 2) A series of irregular fractures not noted previously occur on high and low atmospheric pressure abraded grains. These "popouts", about 5

to 10 μ m in diameter, apparently are the result of violent fracturing of grain surfaces, they probably represent very energetic, rare collisions. More of these features occur on grains abraded at low than high atmospheric pressures.

3) Other features that are rather rare and noticeable at high magnification are irregular surface fractures, these features generally are 5 to 50 μ m long. Further abrasion of grains with cracks may lead to spalling of portions of grain surfaces. The few cracks that were observed were noted on the "low pressure" grains rather than the "high pressure" samples.

4) Rounding occurs much more rapidly in the low than the high atmospheric pressure environment. The process of rounding is due to the abrasion of irregular fracture patterns on freshly crushed Brazilian quartz, upturned cleavage plates are formed which eventually cover the grains completely. Tiny rows of plates cover places where large angular areas were present, and at magnifications in which the entire grain is observed, the small plates create the appearance of rounding. Thus rounding simply corresponds to extensive "upturned plate" formation.

5) More conchoidal fractures and fewer "upturned plates" were found on the "low pressure" grains (500-850 μ m diameter grains) than on the "high pressure" ones.

A number of other rather interesting observations were made which did not directly relate to the difference between abrasion of high and low atmospheric pressure.

1) After extended abrasion, the larger grains (at both pressures) were similar to modern aeolian dune sands in terms of degree of rounding and surface texture. The only major differences were those due to lack of solution and precipitation which occurs on Earth deserts. This suggests that the abrasion experiments at least roughly approximated aeolian desert abrasion.

2) The larger grains were better rounded after 3 hours than the smaller ones after 8 hours at both high and low atmospheric pressures, probably because of the increased momentum associated with the larger ones.

3) Spacing of "upturned plates" on small grains abraded at low pressures appears to be closer than on those abraded at high pressures. This may have occurred because of the greater number of collisions and greater momentum generated at low pressures.

In summary, abrasion under low atmospheric pressures appears to occur more rapidly, and creates somewhat more irregularities on grain surfaces than at high atmospheric pressures characteristic of Earth. The frequency of certain types of breakage textures appears to be more common in low pressure environments than in high pressure environments. Thus the differences so far observed are mostly of degree rather than of kind and may be the result of decreased air cushions between grains at low pressures as suggested by McCauley (1973). However, it should be noted that wind velocities of only 8 meters per second were used in wind tunnel experiments,

while maximum velocities presumed for wind storms on Mars may be as much as ten times that figure

A number of quartz particles, perhaps on the order of a micron in diameter or less, appear to have been partly melted. This was observed on grains that had been abraded at only 8 meters per second, the effect on quartz and basalt sand grains at velocities ten times as high is unknown. It may be that the "partly melted" material is a different phase from the original quartz structures, perhaps more poorly crystalline.

Angular particles less than a micron in diameter are observed in great numbers adhering to the surfaces of large grains abraded at both high and low pressures, they are extremely difficult to remove. This phenomenon is not found on aeolian quartz grains, freshly broken surfaces on the experimental grains react differently than the weathered material. Perhaps electrostatic forces are important here, if crystals are cleaved or split under a vacuum, electron energies of hundreds of kilovolts may be produced (Moore, 1973). It has been suggested that the martian dunes may be composed of aggregates and clods rather than mineral grains and rock fragments (Moore et al., 1977) and electric charging by mechanical fracture of materials could be involved.

REFERENCES CITED

- Krinsley, D., Friend, P., and Klimentidis, R., 1976. Eolian transport textures on the surfaces of sand grains of early Triassic age. *Geol Soc America Bull.*, Vol. 87, pp. 130-132.
- McCauley, J. F., 1973. Mariner 9 evidence for wind erosion in the equatorial and mid-latitude regions of Mars. *J. Geophys. Res.*, Vol. 78, pp. 4123-4137.
- Moore, A. D., 1973. *Electrostatics and its applications*. John Wiley and Sons, New York, p. 84.
- Moore, H. J., Hutton, R. E., Scott, R. F., Spitzer, C. R., and Shorthill, R. W., 1977. Surface materials of the Viking landing sites. *J. Geophys. Res.*, Vol. 82, pp. 4497-4523.

EOLIAN DEPOSITS OF PAIUTE TRAIL POINT, ARIZONA

McCauley, Camilla K. and Augustus S. Cotera, Department of Geology, Northern Arizona University, Flagstaff, Arizona, 86011.

The dynamics of wind-blown sand and dune formation on sloping surfaces are being investigated in a remote area of the Navajo Reservation in northern Arizona. The dune field lies within the region first described by John Hack (1941) in his classic study of the western Navajo Reservation. Within this area, wind-blown sand has accumulated and formed various types of dunes that extend up and over a 200 foot high escarpment below the Moenkopi Plateau. Here the winds are funnelled up a series of former water courses in the cliffs. These notches are now undergoing modification by abrasion and deflation. The object of this study is to attempt to analyze and quantify those factors which influence sand movement and accumulation, and to determine their effects on grain size parameters. Within this dune field, the effect of topography is especially important.

Field investigation shows evidence of at least two separate periods of dune formation. However, examination of grains from three different samples under the scanning electron microscope, shows at least three eolian stages (Le Ribault, personal communication). These earlier periods of dune formation are probably related to climate change, however, the present dune formation may also result from surface destabilization caused by human activities and by the introduction of grazing animals within the last 100 years.

Three portable recording wind systems have been installed at various locations within the dune field, both on top of and below the escarpment. Two of the systems record wind velocity and direction at variable heights up to 33 feet above the surface. This instrumentation enables simultaneous comparison of winds at various locations and elevations. In addition, several types of vertical sand traps are being tested to measure the quantity of sand accumulation at different heights above the ground. By combining these systems it will be possible to measure the effects of different wind velocities on the total amount of sand flow as well as vertical distribution and grain size variations. There has been a long-standing need for such instrumented field studies, as was recently pointed out by Howard, et al (1977).

Seventy samples within the dune field have been analyzed to determine their statistical grain size parameters. In addition, fluvial sand from washes that supply sand to the dune field have also been analyzed for comparison. Preliminary results are shown in Table 1.

TABLE 1. GRAIN SIZE PARAMETERS -- PAIUTE TRAIL POINT DUNE FIELD

| <u>SAMPLE LOCATION</u> | <u>MEAN GRAIN SIZE</u> | <u>SORTING</u> | <u>SKEWNESS</u> | <u>KURTOSIS</u> |
|----------------------------------|------------------------|----------------|-----------------|-----------------|
| Wash sediments | 3.14 ϕ | 1.06 ϕ | 0.14 | 1.49 |
| Dunes below escarpment | 2.13 ϕ | 0.71 ϕ | 0.06 | 1.03 |
| Dunes on top of escarpment | 2.15 ϕ | 0.57 ϕ | 0.09 | 1.02 |
| Falling dunes | 2.24 ϕ | 0.56 ϕ | 0.12 | 1.08 |
| Climbing dunes | 2.30 ϕ | 0.67 ϕ | 0.05 | 1.07 |
| Older dunes below escarpment | 2.64 ϕ | 0.70 ϕ | 0.20 | 1.00 |
| Older dunes on top of escarpment | 2.72 ϕ | 0.80 ϕ | -0.04 | 1.16 |

ORIGINAL PAGE IS
OF POOR QUALITY

Table 1 shows that the active dune sands are generally very similar except for subtly finer grain sizes on the slopes and on the top of the escarpment. The older, stabilized dunes are very much finer grained than any of the other sites. The wash sediments are bimodal in size, poorly sorted and leptokurtic.

Topography plays an important role on thru-going sand systems. Strong local funnelling effects occur in this area which in turn have caused local increases in wind velocity of as much as 50% as measured in the field. Resulting air-borne sand plumes and gravitational cascades combine to form the morphology of climbing dunes and sand ridges on the escarpment periphery.

This area has been subjected to multiple periods of dune formation of unknown age and to episodic sweeping away of eolian deposits during periods of fluvial activity. Archeologic evidence such as datable artifacts found among the dune sands may provide some idea of the rates and intensity of pluvial and eolian cycles within this region.

REFERENCE CITED

- Hack, J. T., 1941, Dunes of the western Navajo country. Geog. Rev., vol. 31, no. 2, p. 240-263.
- Howard, A. D., Morton, J. B., Gal-el-Hak, M. and D. B. Pierce, 1977, Simulation model of erosion and deposition on a barchan dune, NASA CR-2838, 77 p.
- Le Ribault, Loïc, Compagnie Francaise des Petroles, Paris, France, personal communication.

INTERPRETING DUNE DEPOSITS THROUGH MINOR STRUCTURES

McKee, Edwin D , U.S. Geological Survey, Denver, CO 80225.

Steeply dipping, large-scale cross-strata are the most commonly recognized primary structure used to interpret deposits thought to be eolian. These structures, which develop as the slipfaces of dunes, characteristically are large scale (commonly 20 to 40 m long), high angle having a dip of 30° or more), and either tabular planar or wedge planar in form. Almost all of the steeply dipping foresets form tangents with a horizontal base. Statistical studies of the dip directions of cross-strata indicate that mean-direction vectors and the amount of spread in directions are good indicators of the type of dune represented and the direction or directions of wind transport involved.

Despite the importance of cross-strata in the interpretations of dune deposits, large-scale cross-strata may form in several depositional environments; thus, evidence from various minor structures must be evoked in many studies to supplement available data or to confirm an interpretation. Such minor structures may be either primary or penecontemporaneous. They include ripple marks, raindrop impressions, slump marks, various types of contorted beds, and features of preservation in the tracks and trails of animals.

Wind-formed ripple marks, as represented in ancient deposits, are distinctive structures and normally differ from water-formed ripple marks in two essential respects: Eolian ripples are low, wide, and asymmetrical, with ripple indexes (ratio of wave length to amplitude) greater than 15; and they have crests and troughs oriented parallel to the direction of dip of the foreset slopes. Actually, a large majority of ripple marks on modern dunes are formed with horizontal orientation normal to the wind on the gentle windward slopes of saltation, but very few of these windward-side deposits are preserved. Thus, the straight, parallel crests and troughs trending up and down steep slipfaces and buried by avalanching sand constitute the permanent record.

Raindrop impressions in fine sand form small craterlike pits that give positive evidence of subaerial deposition. They form thin detached layers or shells, roughly circular but with irregular margins resulting from cohesion of grains by the introduction of moisture. On sloping surfaces of slipfaces, they become reoriented to the horizontal and each circular pit tends to face upward or vertically, thus raising the downslope rim.

Contorted structures of various types are common features of the slipface deposits of many dunes. Not only are they distinctive and easy to recognize, but they also furnish useful information concerning the part of the slope represented and the degree of cohesion of the sand involved. Eight or more types of deformational structure have been recognized on dune slipface deposits; and, on the basis of these structures, it usually is possible to determine whether the upper part (area of tension) or the lower part (area of compression) is involved. Further, from the type of deformation, the probability that the sand was wet, dry, or saturated, or had a wet crust commonly can be ascertained.

ORIGINAL PAGE IS
OF POOR QUALITY

Very important to the correct interpretation of dune deposits are the closely associated interdune sediments. In vertical sections, interdunes may be a meter or more in thickness, or they may be absent, with their stratigraphic position represented by a prominent bedding plane. Their thickness is primarily a function of the length of time the interdune accumulated sediment before being buried by the advance of steeply dipping dune foresets. The interdunes range from long narrow corridors between sand ridges to rounded, elliptical depressions between mounds of sand. Their deposits contrast with those of enclosing dune foresets in color, composition, bedding type, and sorting; their bases are commonly on truncated planes, slightly curving rather than flat. They may contain coarse-sand or gravel lag, irregular adhesion ripples, and horizontal bedding.

DUST STORMS ON MARS VISUAL AND THERMAL OBSERVATIONS FROM VIKING

Peterfreund, Alan R., Department of Earth and Space Sciences, University of California, Los Angeles, CA 90024.

In 1977, two major dust storms and numerous local ($\sim 10^5$ km²) dust clouds were observed by the visual imaging systems (VIS) and infrared thermal mappers (IRTM) aboard the two Viking orbiters. The storms occurred primarily in the southern spring and early summer, when sublimation of the south polar cap was occurring, Mars was near perihelion, and peak solar insolation at the southern sub-solar latitudes resulted in measured brightness temperatures of over 300 K for some areas at midday. In figure 1, an overview is presented of the occurrences of global and local dust storms versus time in solar longitude (L_s).

The first major dust storm ($L_s = 205$) occurred two and a half months prior to perihelion, which is unusually early for the onset of the global storm according to earth-based observers. The atmospheric opacity slowly decreased to a relatively clear state by $L_s = 250$. At $L_s = 275$ the second major dust storm began. By $L_s = 340$, the atmosphere was again relatively clear. Both storms were first observed in the Thaumasia region, south of the Tharsis Plateau, historically a common location for the origin of global dust storms.

When initially observed, both major storms already covered approximately 10^8 km². Numerous regions of local turbulence, where dust was presumably being raised, were observed in both visual and thermal data. As the storm matured, it became more widespread and turbulent regimes became less common. The decay phase was marked by a slow decrease in visual and thermal opacity.

Atmospheric thermal characteristics observed during the global storms were a marked increase in diurnal amplitude, peaking at 1800 hours and -65° latitude, and a general warming of the atmosphere, particularly noticeable over the north polar region (Martin, 1977). The increase in temperatures over the north pole were almost simultaneous with the initial observations of the storms. This implies a rapid transfer of energy northward in the atmosphere due to suspended dust.

Of the numerous local dust clouds identified from VIS frames and IRTM data, all but two have been in the southern hemisphere. The dust clouds in the north were observed at $L_s = 200$ at 42°N , 142°W and at $L_s = 342$ over the Viking Lander 1 site, 22°N , 48°W . The latter was an exciting observation, since lander data were also available. At the time of this writing much of the data was still unprocessed, but it appears that westerly winds were probably between 20 and 30 m/s, the highest recorded to date (Henry, 1977). The morphologies of both northern storms suggests that they are local in origin. This is significant because the prevailing hypotheses are that season and latitude are important for the generation of local storms.

The local dust clouds in the southern hemisphere observed by the imaging and infrared thermal mapping instruments during the southern spring represented by hexagons and black dots, respectively, in figure 1. Two general classifications based on latitude are apparent, one being those clouds along the edge of the receding south polar cap and the other being those

occurring between -15° and -30 degrees latitude.

The clouds along the receding south polar cap are located in regions where steep surface temperature gradients would probably contribute to the production of winds capable of raising dust. As the south pole receded, this region moved progressively south.

Surprisingly, the local dust clouds in the mid- and low-latitude region of the southern hemisphere were limited to a small range of longitudes. While observations were made of all longitudes, the only region of local dust storm activity was that between 80 and 130 degrees longitude, the same region in which both global dust storms were first identified. The fact that local dust clouds were not observed elsewhere in the southern hemisphere, except near the polar cap edge, was a surprise, since there have been many historical occurrences of clouds in the Hellespontes and Noachis regions at this season.

Apparent motion of seven of the local clouds was derived from sets of diurnal observations. Estimated velocities ranged from 9 to 44 meters per second, with a mean velocity of 22 m/s. The directions of motion show fairly consistent alignment with the prominent wind streaks on the underlying surface. Variable albedo features observed in this region on both Mariner 9 and Viking images suggest local changes have occurred in deposits of fine grained material in relatively short periods of time.

The diurnal characteristics show that the dust clouds are most active in the early part of the day, confirming previous earth-based observations. A particular dust storm at L_s 225 in Solis Planum was observed by the IRTM over a 5.1 hour period starting at local noon, and was found to move with decreasing velocity to the southeast. The following day a VIS observation showed the cloud had either moved back to or regenerated at the original location in the northwest over the intervening 19 hours.

The region in which all the mid- and low-latitude southern dust clouds were observed has a number of unique factors that might combine to produce the necessary conditions for winds capable of raising dust. The area is on the south-southeast slope of the Tharsis uplift. The large regional slope might be conducive to the production of downslope winds; these may originate at night on the abnormally cold flanks of Arsia Mons (Kieffer et al, 1976). The albedo and thermal inertia of this region determined from IRTM measurements, (Kieffer et al, 1977) both exhibit strong local and regional variation. The variation in thermal properties would contribute to the production of local and regional thermal winds. The occurrence of high albedo - low inertia areas surrounding the Claritas Fossae region also suggest the presence of abundant fine-grain material on the surface.

ACKNOWLEDGEMENT:

This work was supported by NASA contract NAS 7-100 at the Jet Propulsion Laboratory, Pasadena, California, and contract 952988 to the University of California at Los Angeles. Additional support was received from the NASA Viking Project Office.

REFERENCES CITED

- Henry, R. M., 1977 Personal communication.
- Kieffer, H. H., P. R. Christensen, T. Z. Martin, E. D. Miner and F. D. Palluconi, 1976. Temperatures of Martian surface and atmosphere Viking observations of diurnal and geometric variations. *Science*, no. 194, pp 1346-1351.
- Kieffer, H. H., T. Z. Martin, A. R. Peterfreund, B. M. Jakosky, E. D. Miner and F. D. Palluconi, 1977. Thermal and albedo mapping of Mars during the Viking primary mission. *J. of geophysical research*, vol. 82, no 28, pp 4249-4291.
- Martin, T. Z., 1977. Mars. Global thermal behavior In proceedings of the planetary atmosphere symposium. Ottawa. In press.

DUST STORMS VIKING 1977

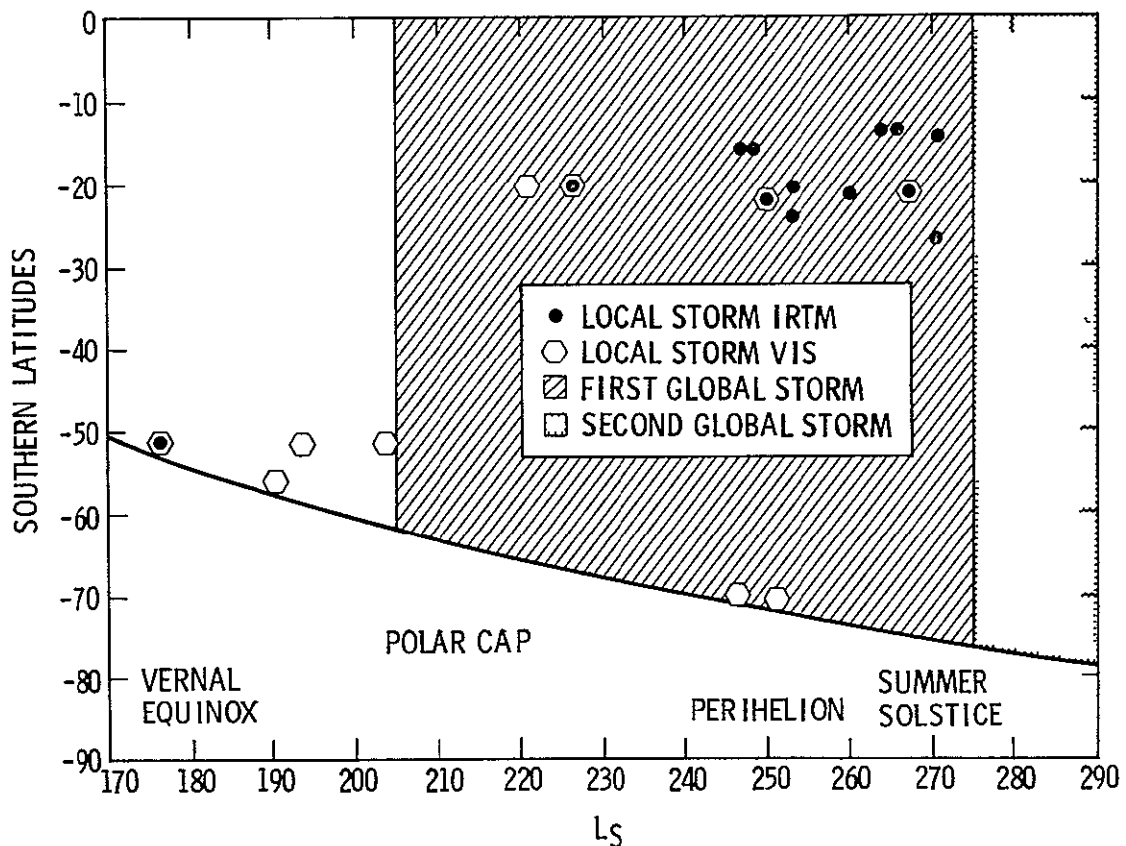


FIGURE 1

ORIGINAL PAGE IS
OF POOR QUALITY

VIKING OBSERVATIONS OF DUST SUSPENDED IN THE MARTIAN ATMOSPHERE

Pollack, J.B., NASA-Ames Research Center, Moffett Field, CA 94035

Observations of the Martian sky taken with the Viking Lander Cameras permit a determination of a number of properties of the dust in the Martian atmosphere and their variation over much of a Martian year. These properties include optical depth, mean size, shape, and composition. Such information helps to define the current mass loading density of dust particles in the atmosphere and leads to estimates of the current rate of formation of sedimentary deposits composed of these particles. It also provides clues about the mechanisms responsible for producing such landforms as the polar layered deposits and the debris mantles.

The optical depth τ of the atmosphere can be directly determined from images of the sun (Pollack *et al.*, 1977). To first approximation, the mass loading density of dust particles, m , is related to τ by

$$(1) \quad m = 2/3 \tau r \rho \sim 8 \times 10^{-5} \tau \text{ gm/cm}^2$$

where ρ is the dust particle's density and r its mean size. m refers to the mass of material in a vertical column that extends throughout the atmosphere and has a horizontal cross sectional area of unity. Representative values of r and ρ (.4 μm and 3 gm/cc) have been used to evaluate the proportionality constant on the far right-hand side of equation (1). Viking observations indicate that throughout the Martian seasons experienced to date (northern hemisphere early summer through early spring) τ always had an appreciable value. τ was 0.3 near the start of the mission, increased to about 1.0 during the fall season, underwent a discontinuous rise to about 3 at the beginning of two global dust storms, and subsided towards 1 during the decay phase of these storms. Thus, on the average, $m \sim 10^{-4} \text{ gm/cm}^2$.

Information on particle size and shape can be derived from an analysis of the variation of sky brightness with angular distance from the sun (Pollack *et al.*, 1977). On the average, the dust particles have a mean radius of about 0.4 μm , but analysis of Mariner 9 IRIS observations suggest that the size distribution is very broad on the large particle side of this mean (Toon *et al.*, 1977). Thus, the suspended dust particles have sizes ranging from about 0.1 to 10 μm , a result consistent with modeling of wind tunnel data (Greeley *et al.*, 1976; Pollack *et al.*, 1976) to define the particle size boundary between suspension and saltation. The particles are also found to have sharp edges and approximately equal dimensions.

Analysis of the absolute value of the sky brightness seen on pictures taken with the 6 narrow band channels leads to a determination of the absorption coefficient of the suspended particles and its variation with wavelength. The presence of a sharp minimum in this coefficient near 0.8 μm wavelength implies that magnetite is the opaque phase, with a fractional abundance on the order of 10%. Consequently, while atmospheric conditions have been sufficiently oxidizing to convert some ferrous iron to ferric iron, as evidenced by the red color of the Martian surface, this process has not fully oxidized all ferrous bearing material.

The deposition rate of suspended dust can be estimated from the above cited mass loading density and the characteristic time period over which the optical depth changes. The latter is on the order of several months. Hence, averaged over the planet, the deposition rate of fine dust equals about 5×10^{-4} gm/cm²/year.

The deposition of suspended dust may not be uniform, but rather may show a strong preference for polar latitudes. Because the dust particles have such a small size, their gravitational settling time is very long. But they may serve as nucleation sites for the condensation of water and carbon dioxide ice. If the resulting dust-ice particle is large enough, it will fall rapidly out of the atmosphere. Only modest growth occurs when water ice forms under typical water vapor conditions, but, in the winter polar regions, quite large CO₂ ice particles can be formed ($\sim 25 \mu\text{m}$ in size) (Pollack *et al.*, 1977). Consequently, both dust and water ice may be preferentially deposited in the polar regions. In places where water ice can survive throughout the year, this deposition can contribute to the construction of polar laminated terrain, while at more equatorial latitudes loess deposits will result. When allowance is made for the obliquity oscillations experienced by Mars, the above scenario can account approximately for the observed positions of the laminated terrain and the debris mantles (Pollack, 1977).

REFERENCES CITED

- Greeley, R., B. White, R. Leach, J. Iversen, and J. Pollack, 1976. Mars. Wind friction speeds for particle motion. *Geophys. res. lett.*, vol. 3, pp 417-420.
- Pollack, J.B., 1977. Climatic change on the terrestrial planets. Submitted to *Icarus*.
- Pollack, J.B., D. Colburn, R. Kahn, J. Hunter, W. Van Camp, C.W. Carleton, and M.R. Wolfe, 1977. Properties of aerosols in the Martian atmosphere, as inferred from Viking lander imaging data. *J. geophys. res.*, Sept. 30 issue.
- Pollack, J.B., R. Haberle, R. Greeley, and J. Iversen, 1976. Estimates of wind speeds required for particle motion on Mars. *Icarus*, vol. 29, pp 395-417.
- Toon, O.B., J.B. Pollack, and C. Sagan, 1977. Physical properties of the particles composing the Martian dust storm of 1971-1972. *Icarus*, vol. 30, pp 663-696.

BARCHAN DUNES: DEVELOPMENT, PERSISTENCE AND GROWTH IN A MULTI-DIRECTIONAL WIND REGIME, SOUTHEASTERN IMPERIAL COUNTY, CALIFORNIA

Smith, Roger S.U., Geology Department, University of Houston, Houston, Texas 77004

Development, persistence and growth of barchan dunes during 1968-76 in a multidirectional wind regime suggest that barchans here are not relics of a former unidirectional wind regime but continue to form and prosper in response to favorable local conditions of sand supply and texture of the underlying surface. Once established, barchan form seems to tolerate adverse wind conditions.

These barchans, 0.5-6m high, occupy a 2.5km², gravel-floored intra-dune flat within the Algodones Dunes. Since 1948, they have migrated towards S60°-65°E. at average rates of about 5m/yr for large dunes and 20m/yr for small dunes. Their regime of sand-moving winds is intermediate between that at Yuma, Az. (20km E), where W, NW & N winter winds are opposed by SSE & SE summer winds, and Imperial, Cal. (70km W), where W & WSW winds predominate and blow longer and stronger than Yuma winds.

The height of 62 barchans was measured in the field during May and June, 1968, and remeasured during January, 1976, using air photos taken 5-68, 2-72 and 1-76 to identify dunes, plot their migration and determine changes in morphology and dune spacing. Thirty-three barchans grew taller (0.1-1.1m), 17 shrank (0.1-1.2m) and 12 retained their height within 0.1m. Height changes seem independent of original dune height, spacing, position or mergence. Some changes may represent seasonal differences, but each barchan migrated far enough to reconstitute its sand mass more than twice. At least 4 small dunes (<1m) vanished, probably by dissipating their sand masses downwind during adverse wind conditions. Other small dunes overtook and joined larger dunes.

New barchans were spawned both from the SE ends of "longitudinal" ridges and from elongate or bulbous horns of existing barchans. Seven 1968 horns became individual barchans by 1976 and 6 grew by 0.3-0.8m.

THE ALGODONES DUNE CHAIN, IMPERIAL COUNTY, CALIFORNIA

Smith, Roger S.U., Geology Department, University of Houston, Houston, Texas 77004

The Algodones dune chain extends 70 kilometers southeastward from the southeast corner of the Salton Sea to the modern floodplain of the Colorado River in Mexico. The main dune mass, about five kilometers wide and 30 to 90 meters tall, is distinct from lower dunes which occupy a narrow band along the chain's northeast flank and part of East Mesa, a triangular area south and west of the chain. The dune chain rises sharply northeastward from East Mesa as a granule-covered ramp surmounted by sinuous "longitudinal" dune ridges which extend up to 20 kilometers in a southeastward direction. The northeastern boundary of the chain is less distinct and regular because it is embayed and fringing dunes encroach upon the main dune mass. The main dune mass constitutes a series of large, complex, coalesced domal and barchanoid dunes whose surface displays extensive development of "peak-and-hollow" topography. Gravel-floored intradune flats separate the larger dune forms. This gravel surface becomes more continuous to the southeast, where it is overlain by large isolated barchanoid dunes ("megabarchans" of Norris and Norris, 1961) and swarms of small barchans (Norris, 1966, Smith, 1970). Dunes on East Mesa and along the northeastern fringe of the chain are mainly low, vegetated, "transverse" and "longitudinal" dune ridges and some poorly developed barchans.

The Algodones dune chain is made of sand ultimately derived from the Colorado River (Merriam, 1969; van de Kamp, 1973). This sand was probably reworked by wind from the beaches of large lakes which formed by intermittent diversion of the Colorado River into the Salton basin during Quaternary time. This sand was blown either eastward onto the dunes from beaches along the west or northeast sides of East Mesa (Brown, 1923; Loeltz et al., 1975) or southeastward from a point source to form an extending dune mass (Norris and Norris, 1961; McCoy et al., 1967).

Winds are more intense and unidirectional to the west of the dunes than to the east. At Imperial and El Centro, 40 to 80 kilometers southwest of the dunes, winds blow principally out of the west and west-southwest, while at Yuma, Arizona, 20 to 80 kilometers southeast of the dunes, they blow out of the west to northwest and north during the winter but are nearly matched in intensity and duration by southeasterly and south-southeasterly summer winds. These relations suggest that potential modern transport of eolian sand decreases eastward across East Mesa. If modern winds are saturated with sand, the Algodones dune chain may grow from sand dropped by sand-laden winds as they decelerate eastward. If similar conditions prevailed in the past, the dune chain may mark the long-term boundary between the contrasting wind regimes now found in the Imperial Valley and at Yuma. Measurements of wind and sand flux across East Mesa are now underway to determine whether the dune chain now forms the boundary between these wind regimes and serves as a regional sink for eolian sand.

REFERENCES CITED

- van de Kamp, P.C., 1973, Holocene continental sedimentation in the Salton basin, California: a reconnaissance: Geol. Soc. America Bull., v. 84, p. 827-848.
- Loeltz, O.J., Irelan, Burdge, Robison, J.H., and Olmsted, F.H., 1975, Geohydrologic reconnaissance of the Imperial Valley, California: U.S. Geol. Survey Prof. Paper 486-K.
- McCoy, F.M., Jr., Nokleberg, W.J., and Norris, R.M., 1967, Speculations on the origin of the Algodones dunes, California: Geol. Soc. America Bull., v. 78, no. 8, p. 1039-1044.
- Merriam, Richard, 1969, Source of sand dunes of southeastern California and northwestern Sonora, Mexico: Geol. Soc. America Bull., v. 80, p. 531-534.
- Norris, R.M., 1966, Barchan dunes of Imperial County, California: Jour. Geology, v. 74, no. 3, p. 292-306.
- _____, and Norris, K.S., 1961, Algodones dunes of southeastern California: Geol. Soc. America Bull., v. 72, no. 4, p. 605-620.
- Smith, R.S.U., 1970, Migration and wind regime of small barchan dunes within the Algodones dune chain, southeastern Imperial County, California: Univ. Arizona: unpub. M.S. thesis, 125 p.

MARS: FROST STREAKS IN THE SOUTH POLAR CAP

Thomas, P., Veverka, J., Campos-Marquetti, R., and Gierasch, P., Cornell University, Ithaca, New York 14853

Viking Orbiter coverage of the spring recession of the South Polar Cap shows numerous streamlined bright features which are associated with craters and which closely resemble wind streaks. Their seasonal variability suggests that these are accumulations of frost and not of sand or dust.

The frost streaks occur between latitudes of 55° and 80° S; most are associated with craters surrounded by relatively smooth terrain. They are visible as bright, elongated inliers in the annual frost cap up to 40 days before the receding cap margin reaches their location. They become more conspicuous as the margin approaches and survive its passage by 10-40 days. Once the margin passes their location they are not as prominent outliers as are accumulations of frost within certain craters, topographic lows and shaded areas.

The streaks probably represent accumulations of wind-blown CO_2 frost, and provide evidence for the effective redistribution of such frost by Martian winds. Their pattern indicates winds to the E and NE, the direction expected for near-surface winds during winter when the frost is accumulating. In southern summer, after the annual frost cap has disappeared, many of the craters which had frost streaks show dark splotches and dark streaks indicating winds to the W and NW, the direction expected for summer circulation. Many of these dark albedo markings have been stable since the time of Mariner 9 (3 Mars years).

CLASSIFICATION OF MARTIAN WIND STREAKS

Veverka, J , Thomas, P , and Bloom, A., Cornell University, Ithaca, New York
14853

Crater-associated wind streaks on Mars can be classified on the basis of their appearance by using the following two criteria

- a) the presence or absence of a source of streak-forming material within the associated crater,
- b) the albedo of the streak relative to its surroundings (bright, dark, mixed tone).

Type I streaks (those with no associated intra-crater deposits) fall into four main categories

Type I(b)· Bright Streaks. By far the dominant streak type on Mars. Concentrated in a latitude belt between 40°N and 40°S, which probably coincides with the equatorial belt of strong systematic winds during southern summer. Bright streak directions are very coherent and reflect the wind pattern expected at this season. These streaks are interpreted as accumulations of high albedo dust trapped downwind of topographic obstacles during major duststorms (not as accumulations of dust deflated from the associated craters). Statistically craters do not seem to be better at producing bright streaks than are isolated hills. Bright streaks are stable in outline and direction on timescales of Martian years.

Type I(sp). South Polar Frost Streaks. Viking Orbiter images of the receding south polar cap show many examples of large bright streaks. Judging from their seasonal variability these streaks represent accumulations of wind-blown CO₂ frost.

Type I(m): Mixed Tone Streaks. These are uncommon bright streaks with dark borders. They occur scattered throughout the belt of bright streaks but marked concentrations occur in Syrtis Major and in Memnonia. Morphologically they are very similar to normal bright streaks and are interpreted as ordinary bright streaks bordered by zones of erosion.

Type I(rd): Ragged Dark Streaks. Occur in clusters, especially near 30°-40°S latitude, where they often indicate an E to W, or NE to SW windflow. They are variable on timescales of days and are interpreted as erosion scars produced by the deflation of bright material from a darker substrate. They are best developed in association with craters, but some do occur in conjunction with ridges and small hills. The distinctive curved, patchy dark streaks common on the East side of Syrtis Major are probably also erosion scars and do not seem to differ fundamentally from the southern hemisphere ragged dark streaks.

Type II streaks (those associated with intra-crater deposits) are all dark in tone and fall into three closely related categories:

Type II(sh):Southern Hemisphere Type. Concentrated in a latitude belt between 40° and 60°S. They tend to be irregular in outline and to emanate from intra-crater splotch deposits. They probably represent accumulations of dark, splotch-forming material deflated from the associated craters.

ORIGINAL PAGE IS
OF POOR QUALITY

CLASSIFICATION OF MARTIAN WIND STREAKS - CON'T

Type II(op): Oxia Palus Type. Very large dark streaks up to 200 km long by 75 km wide, concentrated in the Oxia Palus region. Emanate from dark dune-deposits within large, degraded craters. Many show bright margins and could be classified as mixed in tone.

Type II(cb) Cerberus Type. Streaks similar to those of Type II(op) but concentrated in the Cerberus region. Like the Oxia Palus type they emanate from dark intra-crater deposits, but these deposits do not have dune-like textures. Generally, the Cerberus streaks do not have the prominent bright margins of the Oxia Palus streaks and tend to be much more streamlined than the Type II(sh) streaks.

All Type II streaks are interpreted as deposits of dark material deflated downwind from the associated craters. Type II streaks are not variable on short timescales. No bright streaks of Type II have been identified yet.

WIND TRANSPORT RATES ON MARS

White, B R , University of California, Davis, California 95616 and
R Greeley, University of Santa Clara, Santa Clara, California 95053

The eolian transport of surface material on the planet Mars is determined from results of low-pressure wind-tunnel testing and theoretical considerations. A semi-empirical relation is developed that will estimate the total amount of surface material moving in eolian saltation, suspension, and surface traction. The estimated total mass movement of surface material q per unit width-time on the surface of Mars is

$$q = 2.61 \rho (V_* - V_{*t}) (V_* + V_{*t})^2 / g$$

where ρ is the density of the atmospheric gas, g is the acceleration due to the gravity, V_* and V_{*t} are the friction speed and saltation threshold friction speed respectively. The units of q are grams per centimeter-second. The assumption of a flat surface composed of nearly uniform particle diameter size distribution is made. A change in the mean particle size is accounted for, and will change the threshold friction speed V_{*t} .

A series of wind-tunnel tests were designed to explore the relation between eolian movement of surface material between terrestrial atmospheric pressures and low pressures equivalent of Mars. (A discussion of the wind-tunnel test facility at NASA-Ames Research Center is available in Greeley et al. 1977.) Using the modified-Kawamura (White and Greeley, 1978) a comparison between Earth and Mars can be made.

$$\frac{q_E}{q_M} = \frac{\rho_E (V_* - V_{*t})_M g_M (V_* + V_{*t})_E^2 C_E}{\rho_M (V_* - V_{*t})_E g_E (V_* + V_{*t})_M^2 C_M}$$

where the subscripts E and M refer to Earth and Mars respectively; and C is a constant which varies for changes in pressure and particle Reynolds number. Assuming the ratio of friction speed to threshold friction speed, V_*/V_{*t} is then the same for both Earth and Mars

$$\frac{q_E}{q_M} = \frac{\rho_E g_M (V_{*t})_E^3 C_E}{\rho_M g_E (V_{*t})_M^3 C_M}$$

To duplicate aerodynamic forces for typical conditions on Mars (i.e., temperature of 200 K and surface pressure of 0.75 kPa), the ambient pressure in the wind tunnel should be approximately 23 mb (2.3 kPa). At this value the gas density of the CO₂ on Mars is equal to the gas density of Earth air in the wind tunnel. This creates equivalent dynamic pressures and consequently aerodynamic forces on the particles. Interparticle force equivalence should exist since the ambient pressure is substantially reduced. The effects of gravity, not accounted in wind-tunnel tests, can be adjusted to Mars readily in the modified-Kawamura mass transport equation.

The wind-tunnel test consisted of spreading a 1 cm thick uniform layer of spherical glass bead particles (mean diameter of 0.208 mm) on the wind-tunnel floor. At the end of the test section a material trap was placed. It consisted of two uniform thin plates spaced 10 cm apart aligned parallel with the flow direction. The plates were from the floor to the ceiling of

the wind tunnel. The front end (upstream side) was open to allow air flow to enter freely. The downstream end was sealed with #100 mesh wire to catch the particles yet still allow a sizeable amount of air to pass through so as not to alter the flow field streamlines around the trap. The length of the trap was approximately 1 m long to prevent rebounding particles off the back screen from bouncing out of the trap. The flow field was carefully observed and no unusual flow anomalies were found due to the presence of the trap. Hence, the trap caught suspendable, saltating and surface creeping particles. Thus knowing the width of the trap and time the saltating process was occurring a material flux rate q (grams of material per unit width per unit time) could be calculated.

First the terrestrial case was tested and found to be in agreement with both theories of Kawamura and Bagnold (figure 1). The test was repeated for martian surface conditions (0.75 kPa, 200 K) and the results are shown in figure 1 also. From the wind-tunnel data an empirical value of C_M can be determined which is, $C_M = 2.61$. Also shown on the graph is the modified-Kawamura curve, the agreement with experiment is remarkable. This enables a calculation of the rates of surface material movement to be made for typical surface conditions on Mars. The resulting expression is

$$\hat{q} = \frac{qg}{\rho V_*^3} = 2.61 \left(1 - \frac{V_{*t}}{V_*}\right) \left(1 + \frac{V_{*t}}{V_*}\right)^2$$

This relation should accurately predict the movement of surface material with knowledge of prevailing and threshold friction speeds for typical surface conditions.

The flux of material on Mars is substantially higher than Earth. This increase is due to the existence of typically large pathlengths in the particle's trajectory and also to the reduction of gravity, which cannot be modeled in the wind tunnel. Moreover, the increase in q between the planets, assuming the ratio V_*/V_{*t} is equal, is

$$q_M = \frac{(V_{*t}^3)_M}{(V_{*t}^3)_E} \frac{q_E}{13.5}$$

For instance, the relationship between the movement on Earth compared to Mars, for equal ratios of V_*/V_{*t} of 1.47, would be $q_M/q_E = 6$ or 6 times as great on Mars for 0.2 mm particles.

Comparing the movement rates for similar dynamic conditions, equal ratios of V_*/V_{*t} on the two planets, yields,

$$\frac{q_{MARS}}{q_{EARTH}} = 0.94 \frac{\rho_M g_E V_{*tM}^3}{\rho_E g_{LM} V_{*tE}^3}$$

A direct estimate of flux rates on Mars can be made by employing the obtained result. The results are shown in figure 2. To obtain a numerical value the threshold friction speed must be known. The value of this will of course vary with the changing size of particles, but once known (see Iversen et al. 1976a, 1975) a direct estimate of q_M can be made. For

example assuming a 7.5 mb (0.75 kPa) pressure at 200 K on the Martian surface for V_*/V_{*t} equal to 1.25, the flux rate q would be approximately 0.98 g/(s cm). This is assuming V_{*t} equal to 1.75 m/s. Hence the important parameters in determining the material flux rates are V_*/V_{*t} and the value of V_{*t} .

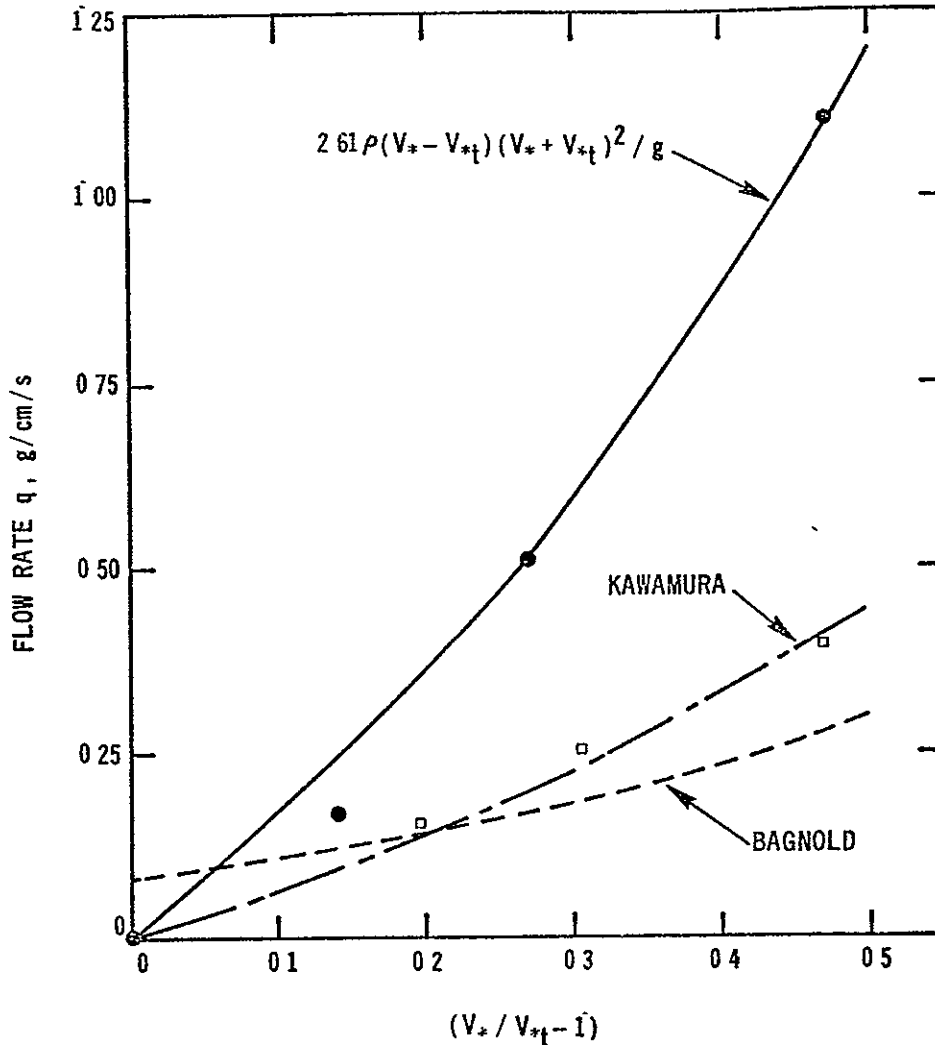


Figure 1 Flow rate q as a function of the parameter $(V_*/V_{*t} - 1)$. The lower two curves represent terrestrial theories of Bagnold (the ---- dashed line) and Kawamura (the — — — solid-dashed line). The hollow square symbols are wind-tunnel data conducted at one atmosphere. Agreement is best when compared to the theory of Kawamura. Bagnold's curve does not predict zero flow rate q at threshold conditions, $(V_*/V_{*t} - 1)$ equal zero. The upper curve (the — solid line) is the modified-Kawamura results taking into account the low-pressure atmosphere and is represented by the expression presented on the graph. The solid circle symbols are low-pressure wind-tunnel data taken in an atmospheric wind tunnel. The agreement between the modified-Kawamura theory and the low-pressure results is excellent.

ORIGINAL PAGE IS
OF POOR QUALITY

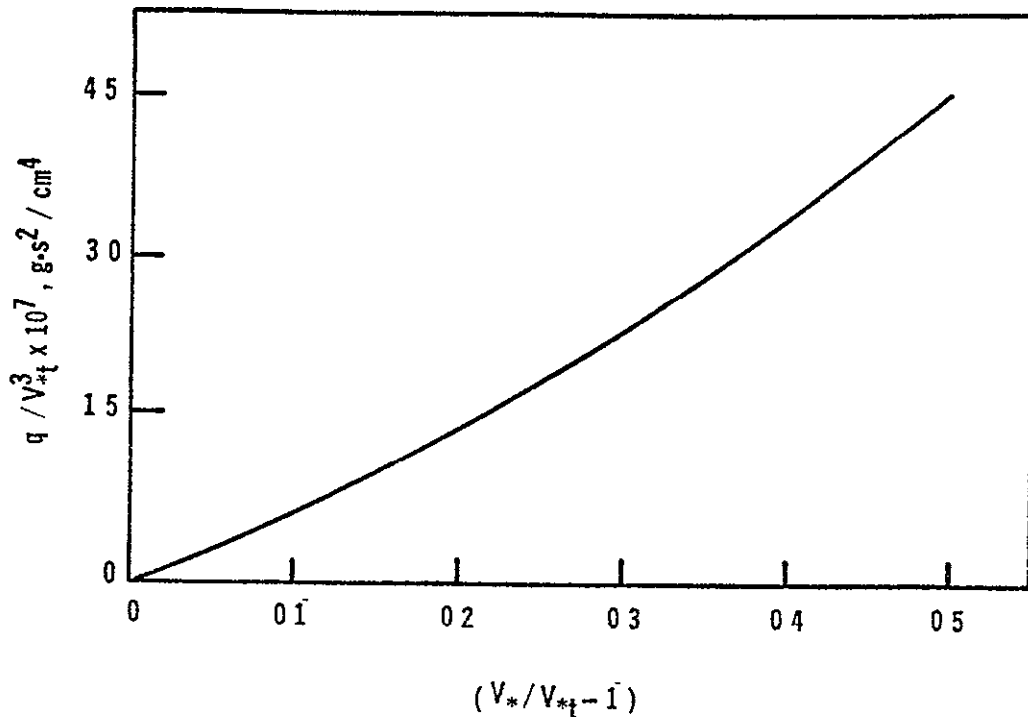


Figure 2 The quantity q/V_{*t} as a function of the parameter $(V_*/V_{*t} - 1)$ for typical martian condition of 7.5 mb (0.75 kPa) pressure, temperature of 200 K and particle densities in the range of 2 to 3 g/cm^3 . Once the value of V_{*t} is known an estimate of the surface material flow rate q can be made from the curve.

REFERENCE CITED

- Bagnold, R. A., 1941 The Physics of Blown Sand and Desert Dunes Methuen and Company, Ltd, London
- Greeley, R., B. R. White, J. B. Pollack, J. D. Iversen, and R. N. Leach, 1977 "Dust storms of Mars: Considerations and simulations" Proceedings of the Desert Dust Symposium, (T. J. Péwé, ed.), American Association of Science, in press.
- Iversen, J. D., R. Greeley, J. B. Pollack, and B. R. White, 1976a "Saltation threshold on Mars: The effect of interparticle force, surface roughness, and low atmospheric density" Icarus, vol. 29, pp 381-393
- Iversen, J. D., R. Greeley, B. R. White, and J. B. Pollack, 1975 "Aeolian erosion on the martian surface: Part I: Erosion rate similitude". Icarus, vol. 26, pp 321-331
- Kawamura, R., 1951. "Study of Sand Movement by Wind" Report, Technical Research Institute, Tokyo Univ., vol. 5, pp 95-112 (in Japanese), also available translated, Univ of Cal., Hydraulic Engineering Laboratory, Wave Research Projects, Technical Report HEL-2-8, 1964
- White, B. R., R. Greeley, 1978 "Wind transport rates on Mars" Journal of Geophysical Research (submitted to).

WAKE OF A THREE-DIMENSIONAL DISTURBANCE IN A TURBULENT BOUNDARY LAYER

White, Bruce R., University of California, Davis, CA 95616, James D Iversen, Iowa State University, Ames, Iowa 50010, and Rodman N. Leach, University of Santa Clara, Santa Clara, California 95053

Three-dimensional velocity measurements of a flow field about a surface disturbance entirely immersed in a turbulent boundary layer have been made. An environmental-atmospheric wind tunnel was used thus developing a naturally turbulent boundary layer. The disturbance within the boundary layer was a stylized model of a volcanic or impact crater. Extensive visual and qualitative studies aided in the interpretation of the complicated viscous interactions occurring in the wake of the model. A characteristic horseshoe vortex was created around the front leading edge of the disturbance and wrapped around sides and extended downstream of the disturbance. In addition to the primary horseshoe vortex system secondary vortex flows are believed to be induced by the primary one, however, the strength of the secondary vortices are small in comparison to the primary one making them hard to observe or measure. A detailed study of the surface pressure distribution was made on the disturbance and surrounding surface area. A strong reverse flow was discovered atop and inside the model crater. Cross-flow (vorticity) was measured in the wake.

There are two types of disturbances that exist in a flow field. One is with the presence of the so-called "large scale" disturbance, which is typically of a larger scale than the boundary layer height, and the second is "small scale" disturbance. In the case of the "small scale", the disturbance of the flow field is contained within the boundary layer. The main difference between these is the small scale disturbance has only a local effect on the pressure gradient (Sedney, 1973). For the flow over a model is immersed entirely within the boundary layer the disturbance may be considered small.

To have a good conceptual understanding of three dimensionally disturbed flow fields there are several common elements to all whether or not the boundary layer is laminar or turbulent and regardless of the geometry of the disturbance. In most cases the law of the wall for turbulent boundary-layer flow will break down in the vicinity of the protuberance, but downstream the laws will be valid when the effects of the disturbance have diminished. In the region of the disturbance the flow will experience streamwise vorticity (crossflow). Immediately upstream of the disturbing element one or more vortices are induced. The primary vortex then stretches around the front of the disturbance (in this case, a model of a volcanic or impact crater) and is termed a horseshoe-shaped vortex (Greeley et al 1974) as shown in figure 1. A secondary set of vortices in an opposite sense of the primary pair is believed to exist on the outer side of the axial centerline next to the primary set. Another set of vortices may exist behind the disturbing element. These are closely spaced vortices that originate from the spiral vortex filaments and rise vertically behind the disturbance. The height of the filaments is approximately the same height as the model. Gregory and Walker (1955) were the first to explore this type of phenomenon in laminar flow. These vortices affect the velocity profiles of the flow by redistributing the momentum immediately downstream of the disturbance.

The spanwise velocity profile in such cases was studied by both Tanı et al (1962) and Gregory and Walker. In disturbed three-dimensional flow vorticity stretching, concentration of vorticity upstream and downstream, and viscous effects must all be considered.

Tanı (1968) reports examples of sudden perturbations given to a turbulent boundary layer such as roughness elements, suction, or injections. He concludes that recovery to equilibrium is very rapid near the wall but rather slow in the outer region of the boundary layer.

Although data are limited on three-dimensional flow around a disturbance there are some experimental results that support the existence of the vortex systems. Woo, Peterka, and Cermak (1977) have reported their findings which include the location and description of the horseshoe vortex around cubes and other three-dimensional objects. From the work of A Hiderks, Prandtl (1952) presents pictures of flow around a disturbance exhibiting the horseshoe vortex and two symmetrical spirals immediately downstream of the disturbance. Bensen (1966) also pictorially shows the vortex system's existence for a hemispherical protuberance element. Counihan, Hunt, and Jackson (1974) have deduced an analytical theory for two-dimensional turbulent boundary layer flow for wakes of surface obstacles (also see Hunt 1971, 1973). One of the main shortcomings of analytical theories is they do not adequately describe the distribution of shear stress, including the surface, and turbulent intensity across the wake. This is experimentally attempted in this study with moderate success. Steiger and Bloom (1962, 1963) have examined theoretically three-dimensional flow fields of viscous wakes created from uniform flow. Also, as suggested by Counihan et al (1974), pressure distributions on the obstacle and the surface should be made to test their relation with the wake flow.

The complete understanding of the flow fields around surface obstacles by experimental means is fundamental to a complete solving of analytical problems. Many aspects of the flow field are far too complicated for the analytical theories to handle. The main purpose of this study was to perform an experimental investigation of three-dimensional wakes and flow fields around a surface disturbance.

Three-dimensional mean velocity measurements were made in the wake of a model crater. The detailed measurements of the longitudinal component of mean velocity proved to be the most useful. The measurements of crossflow components of velocity, generally associated with the intensity of vorticity proved to be difficult to obtain as would be expected. An instantaneous picture of the crossflow would be needed to entirely describe the flow field of the wake, however, such complicated measurements are presently not possible. An analysis of the crossflow does not prove useful in obtaining precise instantaneous vorticity measurements. The details of the flow field seemed to be smeared by an unsteady meandering of the vortex systems.

The magnitude of the crossflow was shown to be always less than 10% of the undisturbed value. Only when the vorticity was relatively stable were measurements of the crossflow components of velocity valuable tools for interpreting the flow field. This occurred only close to the disturbance. Even the most sophisticated equipment, such as two- and three-components

laser doppler velocimeters, would be unable to capture an accurate flow field picture without simultaneously measuring the flow field at one instant in time. This is virtually impossible.

The measurements of the mean longitudinal velocity showed the wake to be symmetrical about the centerline. The wake diffused outward and upward slowly as it proceeded downstream. The primary horseshoe vortex system was easily noticeable in the wake velocity measurements. Scales of turbulence from both hot-film measurements and visual tuft observations showed increases in the wake compared to those in the undisturbed flow. Longitudinal mean velocity profiles exhibited a rapid return to near equilibrium flow, but a slow return from then to the fully undisturbed flow.

A calculation of the distribution of the surface shear stress was made by integrating the longitudinal mean velocity profiles. A comparison of the numerical results to previous work showed good qualitative agreement. The results show extremely high shearing rates immediately downstream of the model in the vicinity of the horseshoe vortex system. The experimental determination of surface stress appears to be the only way of determining it. This is one of the main shortcomings of present analytical theories of the disturbed boundary layer. These results were also confirmed by the erosion of surface material placed in high stress areas. This occurred at substantially lower speeds than normally required to move the surface material.

The flow visualization study coupled together with the longitudinal velocity measurements provided the most complete picture of the flow field around the surface disturbance. China clay studies revealed areas of high shearing rates underneath the primary vortex core system. The location and size of the vortices were obtained from these studies. As the turbulent boundary layer passed over the model crater vorticity was concentrated at the stagnation point near the leading surface. The vortex lines were stretched around the model and a streamwise component of vorticity was induced. This is the so-called horseshoe vortex system. This was the primary system that generally induces a secondary vortex system near the primary system rotating in the opposite sense. A strong reversing flow existed inside the model crater.

In conclusion it is evident that considerable additional effort is required in determining the entire flow field. Wind-tunnel testing is viewed as an essential part in an accurate determination of the flows. Theoretical considerations have not yet developed to a state-of-art where they can predict turbulence levels and stress distribution in the disturbed boundary layer flows. The investigation of three-dimensional turbulent boundary layer flows around surface disturbances is still a formidable problem in fluid mechanic research.

FLOW OVER A RAISED RIM CRATER

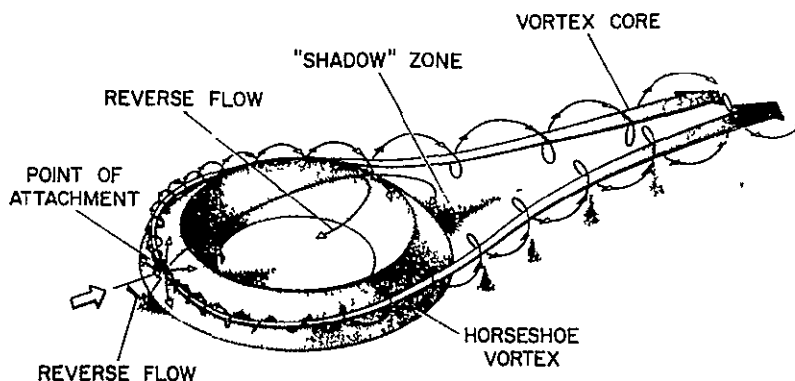


Figure 1 Model crater flow field, showing horseshoe vortex. Longitudinal velocity maxima (shown as vortex cores) of the trailing vortices converge downwind from the model forming a zone of higher surface stress than outside the wake (after Greeley et al , 1974)

REFERENCES CITED

- Benson, B W , 1966 "Cavitation inception on three-dimensional roughness elements" David Taylor Model Basin, Report 2104. Washington, D C.
- Counihan, J , Hunt, J. C R , and Jackson, P S , 1974 "Wakes behind two-dimensional surface obstacles in turbulent boundary layers" Journal of Fluid Mechanics, 64, 529-563
- Greeley, R , Iversen, J. D , Pollack, J B , Udovich, N , and White, B R. , 1974. "Wind tunnel studies of Martian aeolian processes" Proc Roy Soc A , 341, pp 331-360.
- Gregory, N., and Walker, W S , 1955 "The effect of transition of isolated surface excrescences in the boundary layer". R & M 2779. Pt. 1, Aeronautical Research Council, England
- Hunt, J. C R , 1971 "A theory for the laminar wake of a two-dimensional body in a boundary layer" J Fluid Mech., 49, pp 159-178.
- Hunt, J C R , 1973 "A theory of turbulent flow around two-dimensional bluff bodies", J Fluid Mech., 61, pp 625-706
- Prandtl, L , 1952 Essentials of Fluid Dynamics New York, Hafner Publishing Co
- Sedney, R , 1973 "A survey of the effects of small protuberances on boundary layer flow". AIAA J , 11, pp 782-792.
- Steiger, M H and Bloom, M H , 1962 "Three-dimensional viscous wakes" J Fluid Mech., 14, pp. 233-240.

- Steiger, M. H and Bloom, M. H , 1963 "Three-dimensional effects in viscous wakes" AIAA J, pp 776-782
- Tani, I., 1968. "Review of some experimental results on the response of a turbulent boundary layer to sudden perturbation" AFSOR-IFR-Stanford Conference, Vol 1, pp. 483-494
- Tani, I., Komoda, H , Komatsu, Y , and Iuchi, M , 1962 "Boundary-layer transition by isolated roughness". Aeronautical Research Institute, University of Tokyo, Report No. 375,28, No. 7, pp 129-142.
- White, B. R , Iversen, J. D , 1978. "Wake of a three-dimensional disturbance in a turbulent boundary layer" J Fluid Mech. (submitted)
- Woo, H G C , Peterka, J A., and Cermak, J E , 1977 "Wind tunnel measurements in the wakes of structures" NASA CR-2806

APOLLO-SOYUZ OBSERVATIONS OF DESERT ENVIRONMENTS

El-Baz, Farouk, National Air and Space Museum, Smithsonian Institution,
Washington, D C 20560

Experience gained from the Gemini, Apollo and Skylab missions proved that orbiting astronauts could provide valuable data in the form of visual observations and photographs of the Earth. Based on this experience, an experiment was planned on the first international space mission, the Apollo-Soyuz Test Project (ASTP) of July, 1975. One major objective of the experiment was to study parts of the world deserts (El-Baz and Mitchell, 1976). The astronauts concentrated on the description of eolian landforms as well as the effects of the process of desertification. Because color is an important factor in the study of deserts, the experiment included. (1) visual comparisons by the astronauts of terrain color with a "color wheel" composed of 54 Munsell chips; and (2) color photography using specially manufactured film that was processed under controlled conditions for good photographic color balance (El-Baz, 1977)

Most ASTP photographs were taken with a bracket-mounted 70mm Hasselblad camera equipped with a reseau plate. Both 60mm and 100mm Zeiss lenses were used along with an intervalometer for 60% overlap between successive frames. This permitted stereo viewing and the production of controlled photomosaics. A similar 70mm Hasselblad reflex camera was handheld by the astronauts to acquire photographs of selected targets. Both 50mm and 250mm Zeiss lenses were used with this camera. Excellent photographs were obtained of deserts in North Africa, the Arabian Peninsula, Australia, and Argentina. (These photographs are available from the EROS Data Center, Sioux Falls, S. D.) The photography of North Africa is extensive and includes areas of Algeria, Chad, Libya, and Egypt (Figure 1)

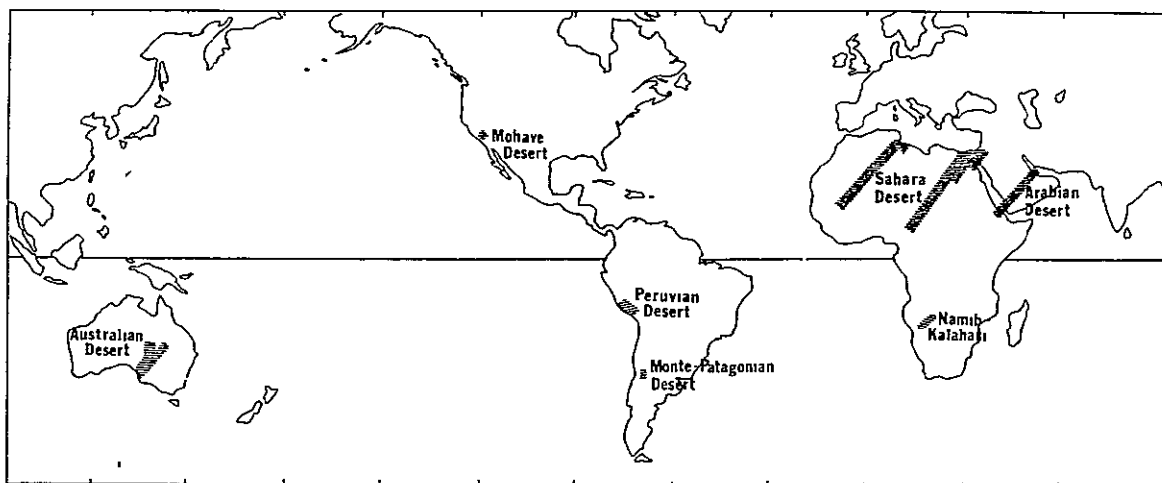


Figure 1. Photographic coverage of desert regions on the Apollo-Soyuz mission. Those of the Peruvian Desert, the Monte-Patagonian Desert, and part of the Australian Desert were taken with the handheld camera. All other strips were taken with the bracket-mounted camera. The author is willing to provide frame numbers of photographs covering specific areas.

ASTP observations indicate that the color of desert surfaces, as seen from orbit, is indicative of soil composition. For example, photographs of the Sturt and Simpson Deserts of Australia show that the sand becomes redder as the distance from the source increases. Field investigations have shown that reddening is caused by a thin iron-oxide coating on individual sand grains (Norris and Norris, 1961, Norris, 1969, Folk, 1976, among others). This reddening may be used to map relative-age zones of photographed areas, particularly in Australia.

Another example of the utility of ASTP color photographs in characterizing desert surfaces is that of distinct color zones in the Western (Libyan) Desert of Egypt. In one photograph (AST-16-1256) taken just west of the Nile Delta, three nearby parallel color zones have been correlated in the field with (1) arable soil composed of quartz sand, clay and calcium carbonate particles, (2) active sand with or without vegetation, and (3) relatively inactive sand mixed with dark (desert-varnished) pebbles (El-Baz, 1978). The youngest yellow sands in this region are in the form of longitudinal dunes, which are migrating to the S-SE along the prevailing wind direction. Identification from orbit of this desert process is significant considering that some of these dunes are encroaching on the western boundary of the fertile Nile Valley. This example shows the importance of these color photographs in identifying both land that is threatened by dune encroachment as well as areas that can be reclaimed from the desert.

These and other examples of Apollo-Soyuz orbital observations strengthen the case for desert study from Earth orbit. Visual observations by well-trained astronauts should be supported by stereo, color and high-resolution photographs on future space missions. The Space Shuttle will allow more detailed study and repeated monitoring of the desert environments in the early 1980's by the use of the 305mm "Large Format Camera".

REFERENCES CITED

- El-Baz, F., 1977. Astronaut observations from the Apollo-Soyuz mission. Smithsonian Institution Press, Wash., D.C., 410pp.
- El-Baz, F., 1978. The meaning of desert color in Earth orbital photographs. Photogram Eng and Remote Sensing (in press).
- El-Baz, F. and Mitchell, D.A., 1976. Earth observations and photography experiment. ASTP Preliminary Science Report TMX-58173, Houston, Texas, pp 10-1 to 10-64.
- Folk, R.L., 1976. Reddening of desert sands. Simpson Desert, N.T. Australia. J. Sed. Petr., vol 46, pp. 604-615.
- Norris, R.M., 1969. Dune reddening and time. J. Sed. Petr., vol 929, pp 81-88.
- Norris, R.M. and Norris, K.S., 1961. Algodones dunes of southeastern California. Geol. Soc. Amer. Bull., vol 72, pp 605-620.

ORIGINAL PAGE IS
OF POOR QUALITY

| | | | |
|---|--|--|---------------------|
| 1 Report No NASA TM-78,455 | 2 Government Accession No - | 3 Recipient's Catalog No | |
| 4 Title and Subtitle ABSTRACTS FOR THE PLANETARY GEOLOGY FIELD CONFERENCE ON AEOLIAN PROCESSES | | 5 Report Date | |
| | | 6 Performing Organization Code | |
| 7 Author(s) Ronald Greeley, Editor* David Black, Coeditor** | | 8 Performing Organization Report No A-7279 | |
| | | 10 Work Unit No 384-50-60-01 | |
| 9 Performing Organization Name and Address *Arizona State University, Tempe, Arizona **Ames Research Center, Moffett Field, Calif. 94035 | | 11 Contract or Grant No | |
| | | 13 Type of Report and Period Covered Technical Memorandum | |
| 12 Sponsoring Agency Name and Address National Aeronautics and Space Administration Washington, D.C. 20546 | | 14 Sponsoring Agency Code | |
| | | 15 Supplementary Notes | |
| 16 Abstract The Planetary Geology Field Conference on Aeolian Processes was organized at the request of the Planetary Geology Program office of the National Aeronautics and Space Administration to bring together geologists working on aeolian problems on Earth and planetologists concerned with similar problems on the planets. Abstracts of papers presented at the conference are arranged herein by alphabetical order of the senior author. Papers fall into three broad categories. 1) Viking Orbiter and Viking Lander results on aeolian processes and/or landforms on Mars, 2) laboratory results on studies of aeolian processes, and 3) photogeology and field studies of aeolian processes on Earth. | | | |
| 17 Key Words (Suggested by Author(s)) Mars geology, Mars sandstorms, Viking results, Aeolian processes, Eolian processes, Sand dunes, California geology | | 18 Distribution Statement Unlimited STAR Category - 42 | |
| 19 Security Classif (of this report) Unclassified | 20 Security Classif (of this page) Unclassified | 21 No of Pages 63 | 22 Price* \$4.50 |